# A glucuronoxylomannan epitope exhibits serotype-specific accessibility and redistributes towards the capsule surface during titanization of the fungal pathogen Cryptococcus neoformans

Probert, Mark; Zhou, Xin; Goodall, Margaret; Johnston, Simon; Bielska, Ewa; Ballou, Elizabeth R; May, Robin

*DOI:*
10.1128/IAI.00731-18



*Document Version*
Peer reviewed version

*Citation for published version (Harvard):*
Probert, M, Zhou, X, Goodall, M, Johnston, S, Bielska, E, Ballou, ER & May, R 2019, 'A glucuronoxylomannan epitope exhibits serotype-specific accessibility and redistributes towards the capsule surface during titanization of the fungal pathogen Cryptococcus neoformans', *Infection and Immunity*, vol. 87, no. 4, e00731. https://doi.org/10.1128/IAI.00731-18

# A glucuronoxylomannan epitope exhibits serotype-specific accessibility and redistributes towards the capsule surface during Titanisation of the fungal pathogen *Cryptococcus neoformans*

Mark Probert[1], Xin Zhou[1], Margaret Goodall[2], Simon A. Johnston[3], Ewa Bielska[1], Elizabeth R. Ballou[1], Robin C. May[1]

[1]Institute of Microbiology & Infection and School of Biosciences, University of Birmingham, Edgbaston, Birmingham, UK. B15 2TT

[2]Institute of Immunology & Immunotherapy, University of Birmingham, Edgbaston, Birmingham, UK. B15 2TT

[3]Department of Infection, Immunity and Cardiovascular Disease and Bateson Centre, University of Sheffield, Sheffield, UK. S10 2TN.

Correspondence to: r.c.may@bham.ac.uk. e.r.ballou@bham.ac.uk
+44-121-4145418 +44-121-414-5572

## Abstract

Disseminated infections with the fungal species *Cryptococcus neoformans* or, less frequently, *C. gattii*, are an important cause of mortality in immunocompromised individuals. Central to the virulence of both species is an elaborate polysaccharide capsule that consists predominantly of glucuronoxylomannan (GXM). Due to its abundance, GXM is an ideal target for host antibodies, and several monoclonal antibodies (mAbs) have previously been derived using purified GXM or whole capsular preparations as antigen. In addition to their application in the diagnosis of cryptococcosis, anti-GXM mAbs are invaluable tools for studying capsule structure. In this study, we report the production and characterisation of a novel anti-GXM mAb, Crp127, that unexpectedly reveals a role for GXM remodelling during the process of fungal Titanisation. We show that Crp127 recognises a GXM epitope in an *O*-acetylation dependent, but xylosylation-independent, manner. The epitope is differentially expressed by the four main serotypes of *Cryptococcus neoformans* and *gattii,* is heterogeneously expressed within clonal populations of *C. gattii* serotype B strains and is typically confined to the central region of the enlarged capsule. Uniquely, however, this epitope redistributes to the capsular surface in Titan cells, a recently characterised morphotype where haploid 5 μm cells convert to highly polyploid cells >10 μm with distinct but poorly understood capsular characteristics. Titans are produced in the host lung and critical for successful infection. Crp127 therefore advances our understanding of cryptococcal morphological change and may hold significant potential as a tool to differentially identify cryptococcal strains and subtypes.

## Introduction

As the two main etiological agents of cryptococcosis, *Cryptococcus neoformans* and *Cryptococcus gattii* are major contributors to the global health burden imposed by invasive fungal infections (1). Whilst *C. neoformans* typically manifests as meningitis in immunocompromised individuals, *C. gattii* infections are not associated with specific immune defects and have been responsible for fatal outbreaks of pneumonia (2–4). Central to the virulence of both species is an elaborate polysaccharide capsule, without which *Cryptococcus* is rendered avirulent (5, 6). The composition of this capsule is highly variable and differs between yeast cells and Titan cells (defined as cells >10 μm in cell body diameter with increased ploidy and altered cell wall and capsule) formed by *C. neoformans* within the host lung (7–9). Titan cells contribute to pathogenesis by resisting phagocytosis, enhancing dissemination of yeast to the central nervous system and altering host immune status (7, 9–13).

The cryptococcal capsule consists of ~90% glucuronoxylomannan (GXM), ~10% glucuronoxylomannogalactan (GXMGal) and <1% mannoproteins (MPs) (14). GXM is a megadalton polysaccharide containing a backbone of α-(1,3)-mannan that is decorated with β-(1,2)-glucuronic acid, β-(1,2)-xylose and β-(1,4)-xylose substituents (15). The backbone mannan can also be *O*-acetylated, although the position at which this modification is added remains unclear for most strains (14–16). Seven repeat motifs – called structure reporter groups (SRGs) – contribute to structural variation in GXM (15). All SRGs contain a β-(1,2)-glucuronic acid on their first mannose residue, however the number of β-(1,2)- and β-(1,4)-xylose substituents varies (15). The extent and position of *O*-acetyl groups in each SRG remain unclear, however xylose and *O*-acetyl groups attached to the same mannose residue appear to be mutually exclusive (17). SRG usage differs between the four main serotypes of

*Cryptococcus*, with each strain designated a serotype based on the reactivity of its capsular material with antibody preparations (18). *C. neoformans* serotypes A and D tend to biosynthesise GXM containing SRGs with fewer xylose substituents than those from *C. gattii* serotypes B and C (15, 19).

Whilst capsule structure differs between serotypes of *Cryptococcus*, a flexible biosynthetic pathway enables rapid remodelling of the capsule under different environmental conditions (20). *In vitro*, changes in *O*-acetylation have been associated with cell ageing in *C. neoformans* (21), reaffirming earlier reports that capsules produced within clonal populations are far from homogeneous (19, 22). *In vivo*, changes in capsule size and structure coincide with the infection of different organs and likely enhance fitness through the evasion of host immunity (23–25). In light of these observations, it is perhaps unsurprising that capsules produced by Titan cells are structurally distinct from those produced by typical yeast cells (7, 11, 26). As the increased chitin content of cell walls produced by Titan cells is associated with activation of a detrimental $T_H2$ immune response during cryptococcosis (27), it is possible that hitherto unidentified structural differences in Titan cell capsules also contribute to the modulation of host immunity by this *C. neoformans* morphotype.

Alterations in capsule structure are likely to affect how *Cryptococcus* is perceived by host immune molecules, with antibodies particularly sensitive to small changes in molecular structures. Following exposure to cryptococci, immunoglobulin M (IgM) antibodies are the most abundant isotype of antibody produced in response to GXM (28). As a repetitive capsular polysaccharide, GXM is a T-independent type 2

antigen and antibodies generated against it utilise a restricted set of variable region gene segments (29). Using monoclonal antibodies (mAbs) in conjunction with mutants harbouring specific defects in GXM modification (17, 30, 31), it has been determined that *O*-acetylation and, to a lesser extent, xylosylation of GXM are important for epitope recognition by anti-GXM antibodies (16, 30). Whilst there is no consensus surrounding the effect of GXM *O*-acetylation on virulence (17, 32), its influence on antibody binding suggests that changes in GXM *O*-acetylation could be a strategy deployed by cryptococci to avoid recognition by immune effectors. Additionally, despite the immunomodulatory roles for GXM *O*-acetylation that have been identified (30, 33), receptors that bind *O*-acetylated GXM remain elusive (34). Due to the enigmatic nature of this modification within the primary virulence factor of cryptococci, further investigation of GXM *O*-acetylation will help unravel the complexities of cryptococcal capsule structure with the ultimate aim of understanding the strategies deployed by this fatal fungal pathogen to evade host immunity.

In the present study, we report the generation of Crp127, a murine IgM mAb, using a cocktail of heat-killed *C. neoformans* H99 (serotype A) (35) heat-killed *C. gattii* R265 (serotype B) (36) and their lysates as an immunogen. Characterisation of Crp127 demonstrated that it is an *O*-acetyl-dependent anti-GXM mAb specific to an epitope expressed by the four *Cryptococcus* serotypes in a serotype-specific manner. Having subsequently found that this epitope is heterogeneously expressed within serotype B populations and is spatially confined to distinct regions of the enlarged capsule across all strains tested, we then turned our attention to its expression by Titan cells. Intriguingly, we noticed that the spatial distribution of this epitope differs within the capsules produced by the three *C. neoformans* morphotypes found within Titanising

populations. Further analysis revealed that, under conditions permissive for Titanisation, cell enlargement coincides with the gradual redistribution of this epitope to the capsule surface.

## Results

### Crp127 recognises a capsular epitope located in GXM

During hybridoma screening, Crp127 was identified as staining the outer zone of live cryptococci. We first assessed whether Crp127 recognises a capsular component by performing flow cytometric analysis of three GXM-deficient mutants (R265 *cap10*Δ (37), KN99α *cap59*Δ (38) and B3501 *cap67*Δ (39)), a GXMGal-deficient mutant (KN99α *uge1*Δ (38)) and a mutant lacking both GXM and GXMGal (KN99α *cap59*Δ*uge1*Δ (38)), using an Alexa-488-conjugated anti-IgM secondary antibody to label Crp127. Unlike their corresponding wild-type strains, the GXM-deficient mutants were not recognised by Crp127 (fig. 1A-C; *cap10*Δ $P < 0.05$; *cap67*Δ $P < 0.01$; *cap59*Δ $P < 0.01$; *cap59*Δ*uge1*Δ $P < 0.01$, Student's t-test). In contrast, the GXMGal-deficient *uge1*Δ mutant was bound at levels similar to the wild-type strain (fig. 1C; $P > 0.05$). Confocal microscopy corroborated these observations, with no observable binding of Crp127 to GXM-deficient mutants but clear binding of Crp127 to the GXMGal-deficient mutant (fig. 1D-F). Taken together, these experiments demonstrated that the epitope recognised by Crp127 – hereon referred to as the Crp127 epitope – is a component of GXM.

### GXM *O*-acetylation is required for Crp127 epitope recognition

Considering the importance of *O*-acetylation and xylosylation to the antigenic signature of GXM (30), we proceeded to investigate the effect of these modifications

on Crp127 epitope recognition. We firstly tested the ability of Crp127 to recognise two xylose-deficient mutants (JEC155 *uxs1*Δ (serotype D) (41) and KN99α *uxs1*Δ (serotype A) (38)). No significant differences were found between either *uxs1*Δ mutant and their corresponding wild-type strains (fig. 2A; JEC155 *uxs1*Δ $P > 0.05$; KN99α *uxs1*Δ $P > 0.05$), indicating that xylosylation does not impact Crp127 binding. In contrast, however, antibody binding was completely abrogated in the *O*-acetyl-deficient *cas1*Δ mutant (fig. 2B; $P < 0.01$), indicating that *O*-acetylation of GXM is an essential prerequisite for Crp127 epitope recognition.

Having made this observation, we proceeded to test two further mutants in genes implicated in GXM *O*-acetylation. KN99α *cas3*Δ exhibits a ~70% reduction in GXM *O*-acetylation, whereas KN99α *cas31*Δ exhibits subtle differences in sugar composition of GXM but no reduction in GXM *O*-acetylation (42). Binding of Crp127 to the *cas3*Δ mutant was slightly reduced but statistically to the wild-type strain (fig. 2C; $P > 0.05$). This may reflect reduced density of *O*-acetylation in GXM produced by this mutant. Surprisingly, however, Crp127 completely failed to recognise the *cas31*Δ mutant despite this strain retaining an *O*-acetylation profile similar to the wild-type (42) (fig. 2C; $P < 0.01$). To be certain that the *O*-acetyl-defective mutants tested still produced capsule, we confirmed the binding of *O*-acetyl-independent anti-GXM mAb F12D2 (43, 44) to each strain (fig. 2K). Thus, *CAS1* and *CAS31* contribute to the formation of an *O*-acetylation dependent Crp127 epitope.

**_Cryptococcus_ serotypes differ in their level of Crp127 epitope recognition**

Differences in the *O*-acetylation state of GXM contributes towards serotype classification and is a source of structural variation within the capsule of cells from a

clonal population (21, 30). Therefore, with Crp127 recognising an *O*-acetyl-dependent epitope, we next checked for differences in Crp127 staining between the five recognised serotypes of *Cryptococcus neoformans* and *gattii*, testing two independent strains of each serotype. Flow cytometry analysis demonstrated that Crp127 consistently bound most effectively to serotype D strains (B3501 and JEC155) (fig. 3A-B), with all cells within these populations exhibiting high-level accessibility of the Crp127 epitope (fig. 3F). We detected slightly lower binding to serotype A strains (fig. 3A-B), with high-level homogeneous staining also seen in the case of H99, but a proportion of unstained cells from strain KN99$\alpha$ (fig. 3C). Interesting, the two AD hybrid strains tested (CBS 950 (47) and ZG287 (48)) were notably different in regard to Crp127 binding (fig. 3A-B), with CBS 950 exhibiting low-level heterogeneous staining and ZG287 showing high-level homogeneous staining (fig. 3G).

The two remaining cryptococcal serotypes, B and C, together represent *C. gattii*. Serotype B strains R265 and CDCR272 (36) demonstrated significantly lower epitope recognition than *C. neoformans* serotypes (fig. 3A-B) and considerable heterogeneity within the population (fig. 3D). Interestingly, however, serotype C strains were completely unrecognised by Crp127, with neither strain CBS 10101 (49) or M27055 (50) showing detectable staining (fig. 3A, B and E). From this, we conclude that there are serotype-specific differences in the availability of the Crp127 epitope, with epitope accessibility being related to serotype in a pattern of D > A >> B >>> C.

**Crp127 exhibits serotype-specific binding patterns that are not associated with opsonic efficacy**

Having identified differential levels of the Crp127 epitope between serotypes using flow cytometry, we next examined their patterns of binding by immunofluorescence microscopy. Indirect immunofluorescence revealed an annular binding pattern for all four strains representing serotypes A and D (fig. 4A and D). In line with their differences in flow cytometry, the two AD hybrid strains tested showed different patterns of binding, with CBS 950 showing punctate binding and ZG287 showing a mix of annular and punctate staining. Both *C. gattii* serotype B strains exhibited punctate binding (fig. 4B and E) whilst, in agreement with flow cytometry, no Crp127 binding was detected when imaging serotype C strains CBS 10101 or M27055. However, *O*-acetyl-independent mAb F12D2 bound well to these strains, suggesting that the lack of Crp127 binding reflects changes in GXM *O*-acetylation rather than loss of capsular material (fig. 4F).

As annular and punctate binding patterns have been associated with opsonic and non-opsonic anti-GXM IgM mAbs, respectively, we tested the ability of Crp127 to opsonise cells from strains KN99$\alpha$ (annular) and R265 (punctate). Unlike positive control treatments mAb 18B7 and pooled human serum, Crp127 did not enhance phagocytosis of either strain by J774 macrophage-like cells in the presence or absence of serum (fig. S2). In summary, annular binding patterns are associated with the high-level binding of Crp127 to *C. neoformans* serotypes A and D strains. On the other hand, punctate binding is associated with low-level binding of Crp127 to serotype B strains. However, under the conditions tested in this study, neither binding pattern is clearly associated with opsonic efficacy.

## Crp127 epitope recognition reflects serotype differences within *C. gattii*

Our data above indicate that Crp127 binding accurately reflects known serotyping of cryptococcal strains. However, recent genomic data indicate that *C. gattii* may in fact be composed of several cryptic species (51). We therefore extended our analysis of this species group by investigating a further four *C. gattii* strains, representing molecular subtypes VGI-VGIII. Similar levels of Crp127 epitope recognition was seen for serotype B strains R265 (VGIIa), CDCR272 (VGIIb), EJB55 (VGIIc) (52) and CA1873 (VGIIIa) (53) (fig. 5A-B; $P > 0.05$), however significantly higher recognition was seen for the serotype B strain DSX (VGI) (54) (fig. 5A-B; $P < 0.01$). Indirect immunofluorescence corroborated these findings, with punctate binding seen for the four strains presenting the epitope at low levels (fig. 5D-H) and annular binding seen for strain DSX (fig. 5C). We also tested strain CA1508 (VGIIIb) (55), a *C. gattii* strain that, to our knowledge, has not previously been serotyped. Both flow cytometry and indirect immunofluorescence showed that Crp127 did not recognise this strain (fig. 5A and H), implying that it is a serotype C strain. In combination with the data presented in figure 3, our finding that four out of five serotype B strains were bound similarly by Crp127 suggests that availability of this epitope is fairly well conserved within this serotype.

## The Crp127 epitope localises to spatially confined zones of the enlarged capsule and binding elicits capsular swelling reactions

Having investigated the binding of Crp127 to cells with a small capsule, we next wished to investigate cells that had been grown in capsule-inducing conditions, given that capsule enlargement occurs shortly after infection of the host. Interestingly, in all

of the strains tested we saw that the Crp127 epitope was spatially confined to distinct capsular regions (fig. 6). For serotype A strains H99, KN99 (fig. 6A), and CBS 8336 (56) (fig. S3F) and serotype D JEC21 and B3501 (fig. 6D) strains, antibody binding was detected in the central zone of the capsule. Serotype B strains differed, with regions adjacent to the cell wall and on the capsule surface bound by Crp127 in the case of strain R265 but only the single region proximal to the surface bound in the case of CDCR272 (fig. 6B). Serotype AD strain ZG287 exhibited a similar pattern of binding to R265, with Crp127 binding to both an inner and outer region of the capsule, however strain CBS 950 was bound in a region adjacent to the cell wall (fig. 6D).

The binding of mAbs to capsular GXM alters the refractive index of the enlarged capsule, resulting in capsular swelling reactions that can be visualised using DIC microscopy (57). In testing the ability of Crp127 to produce a capsular swelling reaction with strains KN99$\alpha$, R265, B3501 and CBS 950, we observed no discernible differences in the reaction pattern produced between strains, with a highly refractive outer rim and a textured inner capsule characteristic for each strain (fig. 6E-H; bottom panels). Notably, however, Crp127 reaction patterns differed from those elicited by 18B7, which also exhibited a highly refractive outer rim but lacked texture throughout the capsule (fig. 6E-H; top right panels). Taken together, our studies of Crp127 binding to capsule-induced cells demonstrate that the Crp127 epitope is localised to specific capsular regions and that Crp127 binding produces capsular swelling reactions that are independent of serotype.

**Spatial distribution of the Crp127 epitope differs within the capsules produced by Titanide, yeast-like and Titan cells**

Following infection of the host lung, a proportion of *C. neoformans* cells differentiate into Titan cells, a very large morphotype that facilitates pathogenesis and is associated with poor clinical outcomes (8, 12). When grown under Titanising conditions *in vitro*, *C. neoformans* forms a heterogeneous population of small, oval-shaped Titanide cells (thin-walled cells 2-4 μm in diameter that are distinct from thick-walled 1 μm micro-cells), yeast-like cells (~5 μm) and large Titan cells (>10 μm) (9, 58). As differences in capsule are known to exist between yeast and Titan cells (26, 59), we tested whether Crp127 could distinguish the morphological subtypes found in Titanising populations from strains H99 and KN99α, two closely-related strains for which Titanisation has been extensively studied (7, 9, 11, 26, 60). Indeed, when these strains were grown under Titanising conditions *in vitro* and imaged, we noticed differences in the spatial distribution of the Crp127 epitope within the capsules produced by cells of different sizes (fig. 7A and fig. S3A). Cells 2-4 μm were poorly recognised by Crp127 (fig. 7A), suggesting these cells did not produce the epitope or that they were had budded after the immunostaining procedure. Crp127 bound to a capsular region adjacent to the cell wall in smaller yeast cells, within the central zone of the capsule in larger yeast-like cells and close to the capsule surface of Titan cells (fig. 7A and fig. S3A). In order to quantify how cell size affects capsular distribution of the Crp127 epitope, we determined the ratio between the area of capsule encompassed by the Crp127 epitope and the area of the whole capsule; using this metric, a ratio approaching 1 is indicative of the epitope being found in close proximity to the capsule surface (fig. 7B). Across three biological repeats (with a mean number of 111 and 133 cells measured for strains H99 and

KN99α, respectively), mean (± standard error of the mean) ratios of 0.07 ± 0.02 and 0.05 ± 0.02 were calculated for cells 2-4 μm in diameter for strains H99 and KN99α, respectively, consistent with our initial observations that Crp127 bound near to the cell wall or not at all in the smallest cells (fig. 7C and fig. S3B). For cells 4-10 μm, mean ratios were 0.42 ± 0.03 and 0.40 ± 0.01 for strains H99 and KN99α, respectively (fig. 7C and fig. S3B), indicating the Crp127 epitope is predominantly located in the central zone of the capsule in 4-10 μm cells, as we had previously observed (fig. 6A). Finally, the mean ratios for cells >10 μm in diameter were 0.72 ± 0.03 and 0.71 ± 0.03 for strains H99 and KN99α respectively, making them significantly higher than those calculated for both 2-4 μm (fig. 7C and fig. S3B; H99 $P < 0.001$; KN99α $P < 0.001$) and 4-10 μm cells (fig. 7C and S3B; H99 $P < 0.001$; KN99α $P < 0.001$). In summary, our results demonstrate that Crp127 binds closer to the capsule surface of Titan cells than Titanide and yeast-like cells in the widely used serotype A strains H99 and KN99α.

**Migration of the Crp127 epitope towards the surface of the capsule coincides with cell enlargement**

To investigate the effect of small changes in cell size on Crp127 epitope distribution, we plotted cell body diameter against epitope proximity to the capsule surface for all H99 and KN99α cells measured (fig. 7D and fig. S3C). In doing so, we identified a positive correlation between cell body diameter and epitope proximity to the capsule surface of yeast-like cells. In agreement with this, when plotting only cells of cell body diameter 4-10 μm, we found a positive correlation between cell body diameter and epitope proximity to the capsule surface in both strains tested (fig. 7E and fig.

S3D; H99 r = 0.65; KN99α r = 0.66). Unlike cell body diameter, capsule diameter did not correlate with epitope proximity to the capsule surface, indicating that changes in capsule size do not explain changes in the proximity of the Crp127 to the capsule surface (fig. 7F and fig. S3E).

Acknowledging the genetic similarities between strains H99 and KN99α, we also investigated serotype A strain CBS 8336 (56), serotype D strain B3501 and serotype B strain R265. Previously, a *C. gattii* strain R265 isolate failed to Titanise *in vitro* using the serum induction protocol, but was observed to form <10 μm Titan-like cells using an alternate protocol (9, 60, 61). Using a different source of R265, we were able to observe limited Titans in this strain using serum induction (Figure S3F). In addition, *C. neoformans* strains CBS 8336 and B3501 both formed Titan cells (Figure S3F). Although Crp127 binding appeared to be redistributed outwards during Titanisation of CBS 8336 and R265, redistribution was less apparent in the case of B3501 (fig. S3F). Thus, the extent of epitope redistribution during Titanisation may vary between strains.

Our results suggest that, in two strains frequently used for the study of Titanisation, the Crp127 epitope moves gradually to the capsule surface as cells enlarge, raising the question of how this may occur. Throughout our imaging experiments, the binding of Crp127 to the majority of Titanide and yeast-like cells (in addition to all Titan cells) produced an annular immunofluorescence binding pattern (fig. 7F; top row). However, we also noticed that some Titanide and yeast-like cells produced a second more faint ring of Crp127 epitope outside of this typical annular ring (fig. 7F; bottom row). This may represent the addition of Crp127 epitope closer to the capsule

surface, partially explaining how redistribution of this epitope coincides with cell enlargement.

## Discussion

In this study, we demonstrated that a capsular epitope recognised by Crp127 – an anti-GXM mAb produced in our laboratory – contributes to serotype-specific differences in capsule structure. This epitope traverses the capsule as cells enlarge under conditions permissive for Titanisation, resulting in its differential distribution throughout the capsule of the three *C. neoformans* morphotypes found within Titanising populations of two strains used to model cryptococcal Titanisation. Detailing the accessibility and localisation of this epitope adds to the existing body of literature surrounding the variability of the cryptococcal capsule between strains and reveals yet another way in which Titan cell capsules are structurally distinct from those produced by yeast cells (21–23, 32, 62).

Based on our examination of a panel of mutants harbouring capsule defects, we propose that Crp127 is an anti-GXM mAb whose binding depends on GXM *O*-acetylation, but not xylosylation. When comparing sequences of the CDRs from Crp127 with four previously characterised anti-GXM IgM mAbs – namely 2D10, 12A1, 13F1 and 21D2 – we found that Crp127 CDRs were significantly different, particularly with regard to the light-chain variable ($V_L$) CDRs. These differences reflect differential gene usage and are likely to manifest as differences in epitope specificity (46, 63). In contrast, when we aligned the heavy-chain variable ($V_H$) and $V_L$ sequences from Crp127 with those from anti-GXM IgG1 mAb 302, we noticed that

390 the sequences were extremely similar as a result of identical variable region gene
391 segment usage by these two mAbs. Identical gene segment usage is not entirely
392 surprising given the restricted set of antibody gene segments utilised by antibodies
393 specific to capsular polysaccharides (29), however the two mAbs were produced in
394 response to GXM derived from different serotypes of *Cryptococcus*. Whereas mAb
395 302 was generated following the immunisation of a mouse with serotype D GXM
396 (ATCC 24064) (64), we generated Crp127 through the immunisation of a mouse with
397 a cocktail containing both serotype A (H99) and serotype B (R265) GXM. Whichever
398 serotype of GXM activated the B cell from which Crp127 derives, the sequence
399 similarities between mAbs Crp127 and 302 demonstrate that nearly identical
400 antibodies can be elicited during infection by at least two different serotypes of
401 *Cryptococcus*.
402
403 Crp127 binding shows strong serotype dependence, with serotype D strains being
404 recognised most strongly, followed by serotype A strains. *C. gattii* serotype B strains
405 show lower, heterogeneous Crp127 epitope recognition and a punctate
406 immunofluorescence binding pattern, whilst serotype C strains entirely fail to bind the
407 antibody. Interestingly, the predominant SRG found in GXM produced by serotype D,
408 A, B and C contains 1, 2, 3 and 4 xylose substituents, respectively (15, 65). Together
409 with the previous observation that β-(1,2)-xylose and *O*-acetyl groups are not added
410 to the same backbone mannose residue (17, 42), this differential SRG usage may
411 explain the variable Crp127 epitope recognition in one of two ways. For example, the
412 additional xylose substituents present in the predominant SRG found in serotype B
413 and C GXM may prevent addition of *O*-acetyl groups in such a way that the Crp127
414 epitope is not formed. Alternatively, the extra xylose substituents found in these

SRGs may sterically hinder binding of Crp127 to its epitope. Studies that further elucidate the roles of specific proteins in GXM biosynthesis – together with advances in techniques that enable chemical synthesis of GXM oligosaccharides – will enhance our understanding of how epitope recognition is achieved by anti-GXM mAbs like Crp127. Intriguingly, a recent transcriptomics study identified *CAS31* as being absent from the genome of strain CBS 10101 (66), a serotype C isolate that we subsequently found was not recognised by Crp127. Whilst we cannot rule out the possibility that other factors contribute to the inability of Crp127 to recognise serotype C strains, it is tempting to speculate that the loss of *CAS31* function in this lineage may explain its lack of reactivity with Crp127 (32, 34). The molecular basis for *CAS31*-dependent epitope recognition remains to be determined, however, the cas31Δ has been shown to harbour minor alterations in GXM xylose composition (38). Therefore xylosylation may be in competition with O-acetylation at Crp127 target residues (17). Consistent with this, anti-GXM mAbs CRND-8, 21D2 and 13F1 also fail to recognise *cas31*Δ mutants (38), suggesting overall changes in capsule organisation in this mutant.

Perhaps our most striking observation regarding the Crp127 epitope was its differential distribution throughout the capsules produced by Titanide, yeast-like and Titan cells of strains H99 and KN99α. Structural differences in Titan capsule compared to yeast capsule have been demonstrated previously by SEM and staining with the anti-capsule antibody 18B7 (7). Additionally, mAb 18B7 staining of *in vivo*-derived Titan cells was heterogenous across individual Titans, including annular, exterior and interior localisations in different cells (7). Using a hypoxic *in vitro* Titan induction protocol, Hommel subsequently showed that there were no differences in

localisation of the anti-GXM mAbs E1, 2D10 or 13F1 in Titans compared to yeast (59). Therefore, the consistent progression in localisation pattern across cell types shown here appears to be a unique feature of the Crp127 epitope (7). The positive correlation between cell size and Crp127 epitope proximity to the capsule surface is suggestive of a scenario whereby the epitope is initially produced in a capsular region adjacent to the cell wall in small Titanide cells before redistributing first to the midzone of yeast-like cells and eventually to the capsule surface of Titan cells. This finding raises the intriguing question of how formation and removal of the Crp127 epitope is so tightly spatially controlled within the capsule. One possibility is that the epitope could be formed at the cell surface and then move outwards as the capsular material elongates. Therefore, we speculate that since the epitope moves outwards at a faster rate than the capsule expands, and since the amount of epitope that initially surrounds a smaller Titanide or yeast-like cell would not be sufficient to form the perimeter of capsule encasing a much larger Titan cell, we instead favour a model in which the epitope is enzymatically removed and added to different regions of the capsule during growth. For instance, it is possible that GXM decorated with *O*-acetyl groups is added closer to the capsule surface in larger cells or that such regions are “unmasked” in a different capsular region as the capsule is reshaped during Titanisation (26).

To summarise, our findings demonstrate that the differential distribution of specific epitopes within the cryptococcal capsule is yet another way in which Titan cells can be distinguished from canonical yeast cells. We hope that this will prompt further investigation into how redistribution of capsular epitopes occurs and what impact this may have on *Cryptococcus* cell biology. We recently showed that Titanisation is

triggered by exposure to components of the bacterial cell wall (9), whilst interactions between bacteria and the capsule have previously been described (67, 68). Capsule also contributes to the buoyancy of *Cryptococcus* cells (69). As such, the importance of redistributing capsular epitopes during Titanisation should be considered in the context of *Cryptococcus* cell biology in both the environment and during infection.

## Materials and methods

### Reagents, strains and mAbs

All reagents were purchased from Sigma-Aldrich unless stated otherwise. The *Cryptococcus* strains used in this study are described in table S1. The anti-GXM mAbs used in this study are described in table S2.

### Growth of cryptococci

*Cryptococcus* strains were preserved at -80°C in MicroBank™ tubes (Thermo Fisher Scientific) prior to being stored on yeast extract peptone dextrose (YPD) agar plates at 4°C for a maximum of 30 days. Unless stated otherwise, strains were cultured on a rotary wheel at 20 rpm for 24 h at 25°C in round-bottom culture tubes containing 3 mL YPD broth. To induce capsule growth, *Cryptococcus* cells were grown in round-bottom culture tubes containing 3 mL Dulbecco's Modified Eagle's Media (DMEM) supplemented with 2 mM L-glutamine, 100 U/mL penicillin, 100 U/mL streptomycin and 10% foetal bovine serum (FBS) for 72 h in an incubator at 37°C and 200 rpm.

### Hybridoma production and mAb purification

Cultures of *C. neoformans* H99 and *C. gattii* R265 were microfuged (4000 x *g* for 5 min) and washed three times in 1 mL Dulbecco's phosphate-buffered saline (PBS). Washed cultures were then heat killed for 60 minutes at 65°C. Following heat killing 20 μL was plated onto YPD to confirm there were no viable cells. Heat-killed H99 and R265 cells were then either lysed (see below) or mixed 1:1 and stored at -20°C prior to inoculation. Fungal cells were lysed using Precellys tubes (UK05 03961-1-004) using programme 6400-2x10-005. Following lysis, lysis beads were microfuged (3000 x *g* for 1 min) and supernatant collected. H99 and R265 lysates were mixed 1:1 and stored at -20°C.

BALB/c mice were hyper-immunised with heat-killed H99 and R265 in addition to their lysates. Hybridomas were generated by a method that has previously been described (70). NS0 immortal fusion partner cells were fused with splenocytes mediated by polyethylene glycol (StemCell Technologies). All animal work was conducted in accordance with Home Office guidelines and following local ethical approval granted under animal licence 30/2788. Supernatants from clones were screened for reactivity with H99 and R265 cells using 96-well plates, with FITC-conjugated anti-mouse IgG and anti-mouse IgM antibodies used to identify positive clones via epifluorescence microscopy. Positive clone 127 was cultured in RPMI 1640 with IgG-depleted FBS and supernatant collected in a MiniPerm bioreactor (Sarstedt). MAb Crp127 was purified from supernatant using affinity chromatography and ProSep Thiosorb (Millipore).

**Hybridoma sequencing and antibody sequence analysis**

514 Sequencing of hybridomas was carried out by Absolute Antibody Ltd (UK).
515 Sequencing was performed by whole transcriptome shotgun sequencing (RNA-Seq).
516 In brief, hybridomas were cultured in Iscove's Modified Dulbecco's Media (IMDM)
517 supplemented with 10% FBS in an incubator at 37°C and with 5% $CO_2$. Total RNA
518 was extracted from cells and a barcoded cDNA library generated through RT-PCR
519 using a random hexamer. Sequencing was performed using an Illumina HiSeq
520 sequencer. Contigs were assembled and annotated for viable antibody sequences
521 (i.e those not containing stop codons) to confirm the species and isotype of mAb
522 Crp127 as murine and IgM, respectively.
523
524 Variable region gene usage was determined using VBASE2 software (71) and CDRs
525 were predicted using the Kabat numbering system (72). Heavy-chain variable ($V_H$)
526 and light-chain variable ($V_L$) sequences of mAb Crp127 were aligned with antibody
527 sequences that have previously been described (40, 73). Amino acid sequences
528 were aligned using Clustal Omega software (74) and annotated using ESpript
529 software (75).
530
531 **Immunolabelling**
532 *Cryptococcus* cells were immunostained for flow cytometry and microscopy
533 experiments. 1 mL of fungal culture was transferred to a 1.5 mL microcentrifuge
534 tube, microfuged (15,000 x *g* for 1 min) and washed 3x in PBS. Cell density was
535 determined using a haemocytometer and adjusted to $10^7$ cells/mL in a final volume
536 of 200 μL. 20 μg/mL Crp127, F12D2, 18B7 or mouse anti-human IgG (IgM isotype
537 control) were added and samples mixed on a rotary wheel at 20 rpm for 1 h at room
538 temperature. Untreated cells for use in flow cytometry were left untreated. After

primary antibody treatment, samples were microfuged (15,000 x *g* for 1 min) and washed 3x in PBS to remove unbound primary antibody. 2 μg/mL Alexa-488-conjugated goat anti-mouse IgM (heavy chain) (Thermo Fisher Scientific), Alexa-647-conjugated goat anti-mouse IgM μ-chain (Abcam) or Alexa-647-conjugated F(ab')2-Goat anti-Mouse IgG (H+L) (Thermo Fisher Scientific) were added to antibody-treated samples and samples mixed on a rotary wheel at 20 rpm for 1 h at room temperature. Secondary antibody was also added to isotype control samples for flow cytometry. For microscopy experiments, 5 μg/mL calcofluor-white (CFW) was also added at this stage to label chitin. Following incubation with secondary antibody, samples were again microfuged (15,000 x *g* for 1 min) and washed 3x to remove unbound secondary antibody and CFW.

**Flow cytometry**

Flow cytometry experiments were performed with an Attune NxT Flow Cytometer equipped with an Attune Autosampler (Thermo Fisher Scientific). Untreated, isotype control and either Crp127 or 18B7 samples were prepared for each strain or conditions tested. Following immunostaining, samples were diluted to 5 x $10^6$ cells/mL and 200 μL of *Cryptococcus* put into individual wells of a plastic round-bottom 96-well plate ready for insertion into the Attune Autosampler. Sample was collected from each well at a rate of 100 μL/min until 10,000 events were recorded. The 488 nm laser was used to detect primary antibody bound by Alexa-488-conjugated secondary antibodies, with the same voltage used to power the laser within each experiment. Flow cytometry data was then analysed using FlowJo (v10) software. Debris was excluded by using the FSC-A vs. SSC-A gating strategy, followed by exclusion of doublets using the FSC-A vs. FSC-H gating strategy (fig.

S4). Exclusion of doublets was used to avoid inclusion of cell aggregates that may happen due to incomplete budding, cell-cell adhesion, or antibody-mediated agglutination. Where GXM-deficient mutants were analysed, samples were only gated to exclude debris due to the inseparable large aggregates formed by these mutants as a result of budding defects. After gating, histograms of fluorescence intensity were plotted and the median fluorescence intensity (MFI) determined. Corrected MFI values were calculated by subtracting the MFI value of the mAb-treated sample by the corresponding isotype control sample in the case of Crp127 or untreated sample where 18B7 was used. Across all experiments, MFI values returned from isotype control cells were extremely similar to those returned from untreated cells.

**Confocal microscopy**

Following the final washes of the immunostaining procedure, 2 μL of stained cryptococcal cells were spotted onto a glass slide and placed under a square glass coverslip. Where visualisation of the capsule was necessary, 2 μL Indian ink was also added to the glass slide. Imaging was performed on a Nikon A1R laser scanning confocal microscope using a 100x object lens and oil immersion. Alongside transmitted light, 639 nm and 405 nm lasers were used to detect Alexa-647-conjugated secondary antibodies and CFW, respectively. For cells with small capsules, Z-stacks spanning 8 μm were generated using steps of 0.27 μm. For capsule-induced cells, Z-stacks were taken across 20 μm using steps of 0.66 μm. Generation of maximum intensity projections (MIPs) and other image processing was performed using NIS-Elements and ImageJ software.

589 **Chemical de-*O*-acetylation of capsular GXM**

590 Where chemical de-*O*-acetylation of the capsule was required, cells were grown in
591 YPD broth that had been adjusted pH 11 with NaOH and sterilised with a 0.22 μm
592 filter. Round-bottom culture tubes containing 3 mL of pH 11 YPD broth was then
593 placed on a rotary wheel turning at 20 rpm for 24 h at 25°C. This method was
594 adapted from that used in a previous study (21).

595

596 **Phagocytosis assays**

597 Phagocytosis assays were performed using the murine macrophage-like J774A.1
598 cell line (mouse BALB/cN; ATCC® TIB-67™). Cells were cultured in DMEM
599 supplemented with 2 mM L-glutamine, 100 U/mL penicillin, 100 U/mL streptomycin
600 and 10% FBS, before 1 x $10^5$ cells were seeded onto round glass coverslips that had
601 been placed into wells of a flat-bottom 24-well plate and incubated for 24 h at 37°C
602 and 5% $CO_2$. Cells of strain R265 and KN99α were opsonised with 18B7 or Crp127
603 as described for the first incubation of the immunostaining procedure. In the same
604 way, cells were opsonised with 10% AB-human serum alone or in combination with
605 Crp127. To achieve a multiplicity of infection (MOI) of 10, $10^6$ R265 or KN99α cells
606 were then resuspended in serum-free DMEM and added to each well of J774A.1
607 cells. Following the infection, each well was gently washed 3x with 1 mL of warmed
608 PBS to remove extracellular yeast. The contents of each well were then fixed with
609 4% paraformaldehyde prior to being washed a further 3x. Cover slips were then
610 extracted from their well, any residual PBS removed by briefly submersing in sterile
611 $dH_2O$ and mounted onto glass slides with Prolong Gold Antifade Mountant (Thermo
612 Fisher Scientific). The total number of internalised yeast cells per 100 J774A.1 cells

(phagocytic index) was determined by microscopic examination using a Nikon TE2000-U microscope with a 60x objective lens and oil immersion.

**Capsular swelling reactions**

Capsule-induced cells were treated with 50 μg/mL Crp127 or 18B7 as described for the immunostaining procedure. 2 μL of *Cryptococcus* cells were then dropped onto a glass slide and placed under a square glass coverslip. Imaging was performed on the differential interference contrast (DIC) channel of a Nikon TE2000-U microscope using a 60x objective lens with oil immersion. Image processing was performed using NIS-Elements and ImageJ software.

**Titan cell experiments**

Titan cells that exhibit all the properties of *in vivo* Titan cells were induced *in vitro* using a previously described protocol (9). *C. neoformans* H99, KN99α, CBS 8336, B3501 and *C. gattii* R265 cells were cultured in glass conical flasks containing 10 mL yeast nitrogen base (YNB) + 2% glucose at 30°C and 200 rpm for 24 h. Cells were adjusted to an $OD_{600}$ reading of 0.001 before being transferred into 10% heat-inactivated foetal calf serum (HI-FCS) at a final volume of 3 mL in a plastic six-well plate and grown for 72 h at 37°C and 5% $CO_2$. To begin a culture derived solely from Titan cells, cells were passed through an 11 μm filter, trapping only larger cells on the filter paper. This filter paper was then washed in PBS to re-suspend Titan cells. Between $10^3$ and $10^4$ Titan cells were then transferred into 3 mL HI-FCS in a plastic six-well plate and cultured for a further 72 h at 37°C and 5% $CO_2$. Titanising populations were prepared for imaging according to the method described for

637 immunostaining. Imaging was performed on a Nikon TE2000-U microscope using a
638 60x objective lens with oil immersion.
639
640 To quantify the proximity of the Crp127 epitope to the capsule surface, ImageJ
641 software was used to draw regions of interest (ROIs) around the cell body, the
642 immunofluorescence binding pattern of the Crp127 and the capsule surface (as
643 determined by Indian ink staining). For each cell measured, the area of these three
644 ROIs was determined before the area of the cell body was subtracted from the areas
645 calculated for both the Crp127 epitope ROI and the capsule surface ROI. Finally, the
646 area of the Crp127 epitope ROI was divided by the capsule surface ROI as a means
647 of quantifying the proximity of the Crp127 epitope to the capsule surface. For cells
648 where no antibody binding was detected, the ratio was scored as 0. A mean number
649 of 111 and 133 cells were measured per biological replicate for strain H99 and
650 KN99$\alpha$, respectively. Image processing was performed using NIS-Elements
651 software.
652
653 **Experimental design and statistical analysis**
654 For each experiment described, three biological repeats were performed as
655 independent experiments that were carried out on different days. All datasets were
656 analysed using GraphPad Prism 7 or 8 software.
657
658 **Acknowledgements**
659 **Provision of antibodies, strains and assistance**
660 We gratefully acknowledge our colleagues Tamara Doering (Washington University),
661 Guilhem Janbon (Institut Pasteur), Arturo Casadevall (Johns Hopkins) and Thomas

Kozel (University of Nevada) providing antibodies and strains and for their invaluable advice regarding this project. We are also grateful to Alessandro Di Maio, Leanne Taylor-Smith and Joao Correia (University of Birmingham) for assistance with confocal microscopy and subsequent image processing.

## Author contributions

Experiments were designed and conducted by MP, XZ and EB. The Crp127 antibody was raised and initially characterised by SAJ and MG. ERB and RCM helped design and oversee this project. Data figures and text were prepared by MP and then edited and revised by all the other authors.

## Competing interests

The authors declare no competing interests with this work.

## Funding

This work was made possible via funding from the Lister Institute for Preventive Medicine and the European Research Council under the European Union's Seventh Framework Programme (FP/2007-2013)/ERC Grant Agreement No. 614562 and from the Biotechnology and Biological Sciences Research Council (BBSRC) via grant BB/R008485/1. RCM is additionally supported by a Wolfson Royal Society Research Merit Award. ZX is supported by a Studentship from the Darwin Trust. ERB is supported by the UK Biotechnology and Biological Research Council (BB/M014525/1) and the Wellcome Trust (211241/Z/18/Z).

**Data and materials availability:** All data needed to evaluate the conclusions drawn in this paper are present in the paper and/or the supplementary materials. Additional data related to this paper may be requested from the authors. The Crp127 antibody described here is available via Ximbio.com.

## References


1. Rajasingham R, Smith RM, Park BJ, Jarvis JN, Govender NP, Chiller TM, Denning DW, Loyse A, Boulware DR. 2017. Global burden of disease of HIV-associated cryptococcal meningitis: an updated analysis. Lancet Infect Dis 17:873–881.
2. MacDougall L, Fyfe M, Romney M, Starr M, Galanis E. 2011. Risk Factors for *Cryptococcus gattii* Infection, British Columbia, Canada. Emerg Infect Dis 17:193–199.
3. Galanis E, Macdougall L, Kidd S, Morshed M, British Columbia Cryptococcus gattii Working Group the BCC gattii W. 2010. Epidemiology of Cryptococcus gattii, British Columbia, Canada, 1999-2007. Emerg Infect Dis 16:251–7.
4. Harris JR, Lockhart SR, Debess E, Marsden-Haug N, Goldoft M, Wohrle R, Lee S, Smelser C, Park B, Chiller T. 2011. Cryptococcus gattii in the United States: Clinical Aspects of Infection With an Emerging Pathogen. Clin Infect Dis 53:1188–1195.
5. Granger DL, Perfect JR, Durack DT. 1985. Virulence of Cryptococcus neoformans. Regulation of capsule synthesis by carbon dioxide. J Clin Invest 76:508–16.
6. Fromtling RA, Shadomy HJ, Jacobson ES. 1982. Decreased virulence in stable, acapsular mutants of cryptococcus neoformans. Mycopathologia 79:23–9.

7. Zaragoza O, García-Rodas R, Nosanchuk JD, Cuenca-Estrella M, Rodríguez-Tudela JL, Casadevall A. 2010. Fungal Cell Gigantism during Mammalian Infection. PLoS Pathog 6:e1000945.
8. Okagaki LH, Strain AK, Nielsen JN, Charlier C, Baltes NJ, Chrétien F, Heitman J, Dromer F, Nielsen K. 2010. Cryptococcal Cell Morphology Affects Host Cell Interactions and Pathogenicity. PLoS Pathog 6:e1000953.
9. Dambuza IM, Drake T, Chapuis A, Zhou X, Correia J, Taylor-Smith L, LeGrave N, Rasmussen T, Fisher MC, Bicanic T, Harrison TS, Jaspars M, May RC, Brown GD, Yuecel R, MacCallum DM, Ballou ER. 2018. The Cryptococcus neoformans Titan cell is an inducible and regulated morphotype underlying pathogenesis. PLOS Pathog 14:e1006978.
10. Okagaki LH, Nielsen K. 2012. Titan cells confer protection from phagocytosis in Cryptococcus neoformans infections. Eukaryot Cell 11:820–6.
11. Crabtree JN, Okagaki LH, Wiesner DL, Strain AK, Nielsen JN, Nielsen K. 2012. Titan cell production enhances the virulence of Cryptococcus neoformans. Infect Immun 80:3776–85.
12. Carter DA, Fernandes KE, Brockway A, Haverkamp M, Cuomo CA, Ogtrop F Van, Perfect JR. 2018. Phenotypic variability correlates with clinical outcome in Cryptococcus isolates obtained from Botswanan HIV/AIDS patients. bioRxiv 418897.
13. Zhou X, Ballou ER. 2018. The Cryptococcus neoformans Titan Cell: From In Vivo Phenomenon to In Vitro Model. Curr Clin Microbiol Reports 1–9.
14. Casadevall A, Coelho C, Cordero RJB, Dragotakes Q, Jung E, Vij R, Wear MP. 2018. The Capsule of Cryptococcus neoformans. https://doi.org/101080/21505594201814310 87.

15. Cherniak R, Valafar H, Morris LC, Valafar F. 1998. Cryptococcus neoformans chemotyping by quantitative analysis of 1H nuclear magnetic resonance spectra of glucuronoxylomannans with a computer-simulated artificial neural network. Clin Diagn Lab Immunol 5:146–59.
16. Cherniak R, Reiss E, Slodki ME, Plattner RD, Blumer SO. 1980. Structure and antigenic activity of the capsular polysaccharide of Cryptococcus neoformans serotype A. Mol Immunol 17:1025–1032.
17. Janbon G, Himmelreich U, Moyrand F, Improvisi L, Dromer F. 2001. Cas1p is a membrane protein necessary for the O-acetylation of the Cryptococcus neoformans capsular polysaccharide. Mol Microbiol 42:453–67.
18. Dromer F, Gueho E, Ronin O, Dupont B. 1993. Serotyping of Cryptococcus neoformans by using a monoclonal antibody specific for capsular polysaccharide. J Clin Microbiol 31:359–63.
19. McFadden DC, Fries BC, Wang F, Casadevall A. 2007. Capsule Structural Heterogeneity and Antigenic Variation in Cryptococcus neoformans. Eukaryot Cell 6:1464–1473.
20. McFadden D, Zaragoza O, Casadevall A. 2006. The capsular dynamics of Cryptococcus neoformans. Trends Microbiol 14:497–505.
21. Gates-Hollingsworth MA, Kozel TR. 2009. Phenotypic heterogeneity in expression of epitopes in the Cryptococcus neoformans capsule. Mol Microbiol 74:126–138.
22. Franzot SP, Mukherjee J, Cherniak R, Chen LC, Hamdan JS, Casadevall A. 1998. Microevolution of a standard strain of Cryptococcus neoformans resulting in differences in virulence and other phenotypes. Infect Immun 66:89–97.

763 23. Rivera J, Feldmesser M, Cammer M, Casadevall A. 1998. Organ-dependent
764 variation of capsule thickness in Cryptococcus neoformans during
765 experimental murine infection. Infect Immun 66:5027–30.
766 24. Charlier C, Chrétien F, Baudrimont M, Mordelet E, Lortholary O, Dromer F.
767 2005. Capsule structure changes associated with Cryptococcus neoformans
768 crossing of the blood-brain barrier. Am J Pathol 166:421–32.
769 25. Garcia-Hermoso D, Dromer F, Janbon G. 2004. Cryptococcus neoformans
770 Capsule Structure Evolution In Vitro and during Murine Infection. Infect Immun
771 72:3359–3365.
772 26. Mukaremera L, Lee KK, Wagener J, Wiesner DL, Gow NAR, Nielsen K. 2018.
773 Titan cell production in Cryptococcus neoformans reshapes the cell wall and
774 capsule composition during infection. Cell Surf 1:15–24.
775 27. Wiesner DL, Specht CA, Lee CK, Smith KD, Mukaremera L, Lee ST, Lee CG,
776 Elias JA, Nielsen JN, Boulware DR, Bohjanen PR, Jenkins MK, Levitz SM,
777 Nielsen K. 2015. Chitin recognition via chitotriosidase promotes pathologic
778 type-2 helper T cell responses to cryptococcal infection. PLoS Pathog
779 11:e1004701.
780 28. Houpt DC, Pfrommer GS, Young BJ, Larson TA, Kozel TR. 1994.
781 Occurrences, immunoglobulin classes, and biological activities of antibodies in
782 normal human serum that are reactive with Cryptococcus neoformans
783 glucuronoxylomannan. Infect Immun 62:2857–64.
784 29. Rohatgi S, Pirofski L-A. 2015. Host immunity to Cryptococcus neoformans.
785 Future Microbiol 10:565–81.
786 30. Kozel TR, Levitz SM, Dromer F, Gates MA, Thorkildson P, Janbon G. 2003.
787 Antigenic and biological characteristics of mutant strains of Cryptococcus

788 neoformans lacking capsular O acetylation or xylosyl side chains. Infect Immun
789 71:2868–75.
790 31. Moyrand F, Klaproth B, Himmelreich U, Dromer F, Janbon G. 2002. Isolation
791 and characterization of capsule structure mutant strains of Cryptococcus
792 neoformans. Mol Microbiol 45:837–849.
793 32. Cleare W, Cherniak R, Casadevall A. 1999. In vitro and in vivo stability a
794 Cryptococcus neoformans glucuronoxylomannan epitope that elicits protective
795 antibodies. Infect Immun 67:3096–3107.
796 33. Ellerbroek PM, Lefeber DJ, van Veghel R, Scharringa J, Brouwer E, Gerwig
797 GJ, Janbon G, Hoepelman AIM, Coenjaerts FEJ. 2004. O-acetylation of
798 cryptococcal capsular glucuronoxylomannan is essential for interference with
799 neutrophil migration. J Immunol 173:7513–20.
800 34. Urai M, Kaneko Y, Ueno K, Okubo Y, Aizawa T, Fukazawa H, Sugita T, Ohno
801 H, Shibuya K, Kinjo Y, Miyazaki Y. 2015. Evasion of Innate Immune
802 Responses by the Highly Virulent Cryptococcus gattii by Altering Capsule
803 Glucuronoxylomannan Structure. Front Cell Infect Microbiol 5:101.
804 35. Perfect JR, Lang SD, Durack DT. 1980. Chronic cryptococcal meningitis: a
805 new experimental model in rabbits. Am J Pathol 101:177–94.
806 36. Kidd SE, Hagen F, Tscharke RL, Huynh M, Bartlett KH, Fyfe M, MacDougall L,
807 Boekhout T, Kwon-Chung KJ, Meyer W. 2004. A rare genotype of
808 Cryptococcus gattii caused the cryptococcosis outbreak on Vancouver Island
809 (British Columbia, Canada). Proc Natl Acad Sci 101:17258–17263.
810 37. Hu G, Kronstad JW. 2006. Gene disruption in Cryptococcus neoformans and
811 Cryptococcus gattii by in vitro transposition. Curr Genet 49:341–350.
812 38. Moyrand F, Fontaine T, Janbon G. 2007. Systematic capsule gene disruption

813 reveals the central role of galactose metabolism on Cryptococcus neoformans
814 virulence. Mol Microbiol 64:771–781.
815 39. Jacobson ES, Ayers DJ. 1979. Auxotrophic mutants of Cryptococcus
816 neoformans. J Bacteriol 139:318–9.
817 40. Casadevall A, DeShaw M, Fan M, Dromer F, Kozel TR, Pirofski LA. 1994.
818 Molecular and idiotypic analysis of antibodies to Cryptococcus neoformans
819 glucuronoxylomannan. Infect Immun 62:3864–72.
820 41. Moyrand F, Klaproth B, Himmelreich U, Dromer F, Janbon G. 2002. Isolation
821 and characterization of capsule structure mutant strains of Cryptococcus
822 neoformans. Mol Microbiol 45:837–49.
823 42. Moyrand F, Chang YC, Himmelreich U, Kwon-Chung KJ, Janbon G. 2004.
824 Cas3p belongs to a seven-member family of capsule structure designer
825 proteins. Eukaryot Cell 3:1513–24.
826 43. Percival A, Thorkildson P, Kozel TR. 2011. Monoclonal antibodies specific for
827 immunorecessive epitopes of glucuronoxylomannan, the major capsular
828 polysaccharide of Cryptococcus neoformans, reduce serotype bias in an
829 immunoassay for cryptococcal antigen. Clin Vaccine Immunol 18:1292–6.
830 44. Brandt S, Thorkildson P, Kozel TR. 2003. Monoclonal antibodies reactive with
831 immunorecessive epitopes of glucuronoxylomannan, the major capsular
832 polysaccharide of Cryptococcus neoformans. Clin Diagn Lab Immunol 10:903–
833 9.
834 45. Casadevall A, Cleare W, Feldmesser M, Glatman-Freedman A, Goldman DL,
835 Kozel TR, Lendvai N, Mukherjee J, Pirofski LA, Rivera J, Rosas AL, Scharff
836 MD, Valadon P, Westin K, Zhong Z. 1998. Characterization of a murine
837 monoclonal antibody to Cryptococcus neoformans polysaccharide that is a

838 candidate for human therapeutic studies. Antimicrob Agents Chemother
839 42:1437–46.
840 46. Casadevall A, Mukherjee J, Devi SJ, Schneerson R, Robbins JB, Scharff MD.
841 1992. Antibodies elicited by a Cryptococcus neoformans-tetanus toxoid
842 conjugate vaccine have the same specificity as those elicited in infection. J
843 Infect Dis 165:1086–93.
844 47. Boekhout T, Van Belkum A, Leenders ACAP, Verbrugh HA, Mukamurangwa
845 P, Swinne D, Scheffers WA. 1997. Molecular Typing of Cryptococcus
846 neoformans: Taxonomic and Epidemiological Aspects. Int J Syst Bacteriol
847 47:432–442.
848 48. Lengeler KB, Cox GM, Heitman J. 2001. Serotype AD strains of Cryptococcus
849 neoformans are diploid or aneuploid and are heterozygous at the mating-type
850 locus. Infect Immun 69:115–22.
851 49. Meyer W, Castañeda A, Jackson S, Huynh M, Castañeda E, IberoAmerican
852 Cryptococcal Study Group the ICS. 2003. Molecular typing of IberoAmerican
853 Cryptococcus neoformans isolates. Emerg Infect Dis 9:189–95.
854 50. Latouche GN, Huynh M, Sorrell TC, Meyer W. 2003. PCR-restriction fragment
855 length polymorphism analysis of the phospholipase B (PLB1) gene for
856 subtyping of Cryptococcus neoformans isolates. Appl Environ Microbiol
857 69:2080–6.
858 51. Hagen F, Khayhan K, Theelen B, Kolecka A, Polacheck I, Sionov E, Falk R,
859 Parnmen S, Lumbsch HT, Boekhout T. 2015. Recognition of seven species in
860 the Cryptococcus gattii/Cryptococcus neoformans species complex. Fungal
861 Genet Biol 78:16–48.
862 52. Byrnes EJ, Li W, Lewit Y, Ma H, Voelz K, Ren P, Carter DA, Chaturvedi V,

Bildfell RJ, May RC, Heitman J, Heitman J. 2010. Emergence and pathogenicity of highly virulent Cryptococcus gattii genotypes in the northwest United States. PLoS Pathog 6:e1000850.

53. Farrer RA, Desjardins CA, Sakthikumar S, Gujja S, Saif S, Zeng Q, Chen Y, Voelz K, Heitman J, May RC, Fisher MC, Cuomo CA. 2015. Genome Evolution and Innovation across the Four Major Lineages of Cryptococcus gattii. MBio 6:e00868-15.

54. Springer DJ, Billmyre RB, Filler EE, Voelz K, Pursall R, Mieczkowski PA, Larsen RA, Dietrich FS, May RC, Filler SG, Heitman J. 2014. Cryptococcus gattii VGIII isolates causing infections in HIV/AIDS patients in Southern California: identification of the local environmental source as arboreal. PLoS Pathog 10:e1004285.

55. Byrnes EJ, Li W, Ren P, Lewit Y, Voelz K, Fraser JA, Dietrich FS, May RC, Chatuverdi S, Chatuverdi V, Heitman J. 2011. A Diverse Population of Cryptococcus gattii Molecular Type VGIII in Southern Californian HIV/AIDS Patients. PLoS Pathog 7:e1002205.

56. Dromer F, Fell JW, Hop WCJ, Theelen B, Diaz M, Meyer W, Abeln ECA, Boekhout T. 2001. Hybrid genotypes in the pathogenic yeast Cryptococcus neoformans. Microbiology 147:891–907.

57. Mukherjee J, Cleare W, Casadevall A. 1995. Monoclonal antibody mediated capsular reactions (Quellung) in Cryptococcus neoformans. J Immunol Methods 184:139–43.

58. Kress Y, Feldmesser M, Casadevall A. 2001. Dynamic changes in the morphology of Cryptococcus neoformans during murine pulmonary infection. Microbiology 147:2355–2365.

888 59. Hommel B, Mukaremera L, Cordero RJB, Coelho C, Desjardins CA, Sturny-
889 Leclère A, Janbon G, Perfect JR, Fraser JA, Casadevall A, Cuomo CA,
890 Dromer F, Nielsen K, Alanio A. 2018. Titan cells formation in Cryptococcus
891 neoformans is finely tuned by environmental conditions and modulated by
892 positive and negative genetic regulators. PLOS Pathog 14:e1006982.
893 60. Trevijano-Contador N, de Oliveira HC, García-Rodas R, Rossi SA, Llorente I,
894 Zaballos Á, Janbon G, Ariño J, Zaragoza Ó. 2018. Cryptococcus neoformans
895 can form titan-like cells in vitro in response to multiple signals. PLOS Pathog
896 14:e1007007.
897 61. Zhou X, Ballou ER. 2018. The Cryptococcus neoformans Titan Cell: From In
898 Vivo Phenomenon to In Vitro Model. Curr Clin Microbiol Reports 5:252–260.
899 62. Fries BC, Taborda CP, Serfass E, Casadevall A. 2001. Phenotypic switching
900 of Cryptococcus neoformans occurs in vivo and influences the outcome of
901 infection. J Clin Invest 108:1639–48.
902 63. Mukherjee J, Scharff MD, Casadevall A. 1992. Protective murine monoclonal
903 antibodies to Cryptococcus neoformans. Infect Immun 60:4534–41.
904 64. Eckert TF, Kozel TR. 1987. Production and characterization of monoclonal
905 antibodies specific for Cryptococcus neoformans capsular polysaccharide.
906 Infect Immun 55:1895–9.
907 65. Janbon G. 2004. Cryptococcus neoformans capsule biosynthesis and
908 regulation. FEMS Yeast Res 4:765–771.
909 66. Farrer RA, Ford CB, Rhodes J, Delorey T, May RC, Fisher M, Cloutman-Green
910 E, Balloux F, Cuomo CA. 2018. Transcriptional heterogeneity of Cryptococcus
911 gattii VGII compared with non-VGII lineages underpins key pathogenicity
912 pathways. bioRxiv 396796.

913 67. Abdulkareem AF, Lee HH, Ahmadi M, Martinez LR. 2015. Fungal serotype-
914 specific differences in bacterial-yeast interactions. Virulence 6:652–657.
915 68. Saito F, Ikeda R. 2005. Killing of *Cryptococcus neoformans* by *Staphylococcus*
916 *aureus* : the role of cryptococcal capsular polysaccharide in the fungal-bacteria
917 interaction. Med Mycol 43:603–612.
918 69. Vij R, Cordero RJB, Casadevall A. 2018. The Buoyancy of Cryptococcus
919 neoformans Is Affected by Capsule Size. mSphere 3:e00534-18.
920 70. Galfrè G, Milstein C. 1981. [1] Preparation of monoclonal antibodies:
921 Strategies and procedures. Methods Enzymol 73:3–46.
922 71. Retter I, Althaus HH, Münch R, Müller W. 2004. VBASE2, an integrative V
923 gene database. Nucleic Acids Res 33:D671–D674.
924 72. Wu TT, Kabat EA. 1970. An analysis of the sequences of the variable regions
925 of Bence Jones proteins and myeloma light chains and their implications for
926 antibody complementarity. J Exp Med 132:211–50.
927 73. Nakouzi A, Valadon P, Nosanchuk J, Green N, Casadevall A. 2001. Molecular
928 basis for immunoglobulin M specificity to epitopes in Cryptococcus neoformans
929 polysaccharide that elicit protective and nonprotective antibodies. Infect Immun
930 69:3398–409.
931 74. McWilliam H, Li W, Uludag M, Squizzato S, Park YM, Buso N, Cowley AP,
932 Lopez R. 2013. Analysis Tool Web Services from the EMBL-EBI. Nucleic Acids
933 Res 41:W597–W600.
934 75. Robert X, Gouet P. 2014. Deciphering key features in protein structures with
935 the new ENDscript server. Nucleic Acids Res 42:W320–W324.
936
937

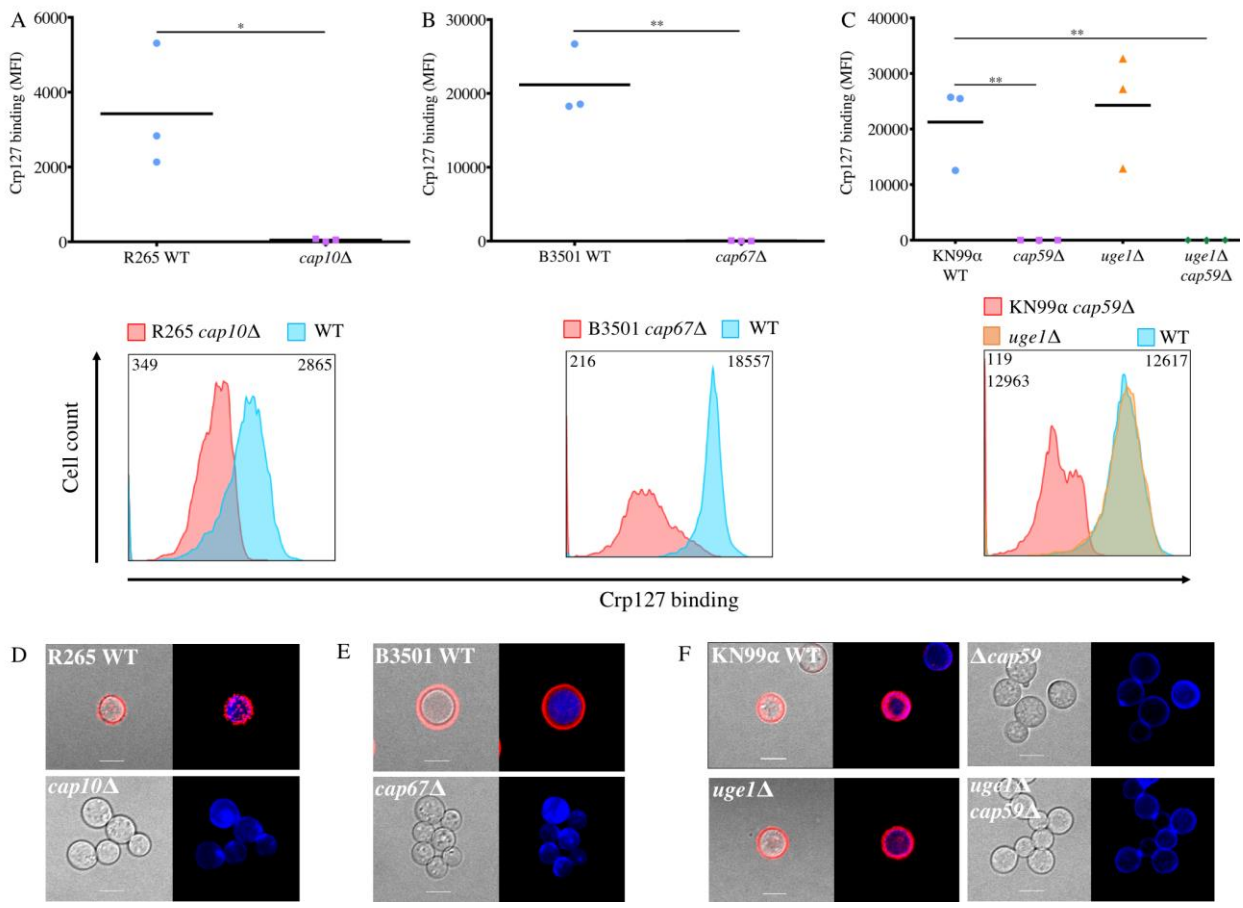
A
Crp127 binding (MFI)
6000
4000
2000
0
*
R265 WT
cap10Δ
B
Crp127 binding (MFI)
30000
20000
10000
0
**
B3501 WT
cap67Δ
C
Crp127 binding (MFI)
40000
30000
20000
10000
0
**
**
KN99α WT
cap59Δ
uge1Δ
uge1Δ cap59Δ
R265 cap10Δ
WT
349
2865
B3501 cap67Δ
WT
216
18557
KN99α cap59Δ
uge1Δ
WT
119
12963
12617
Cell count
Crp127 binding
D
R265 WT
cap10Δ
E
B3501 WT
cap67Δ
F
KN99α WT
uge1Δ
Δcap59
uge1Δ
cap59Δ

***Fig. 1. Crp127 is an anti-GXM mAb.*** *The ability of Crp127 to bind to GXM- and GXMGal-deficient mutants of C. gattii and C. neoformans was quantified via flow cytometry. Scatter plots (top row) and representative histograms (bottom row) are presented for* ***A)*** *R265 cap10Δ,* ***B)*** *B3501 cap67Δ,* ***C)*** *KN99α cap59Δ, KN99α uge1Δ, KN99α cap59Δuge1Δ and their corresponding wild-type strains. For scatter plots, corrected median fluorescence intensity (MFI) values were calculated by subtracting the MFI value of isotype control cells from the MFI value of the Crp127-treated cells, with data points representing MFI values calculated from three biological replicates performed as independent experiments. A Student's t-test was used to test for statistically significant differences between R265 cap10Δ and B3501 cap67Δ and their corresponding wild-type strains, whilst one-way ANOVA followed by Dunnett's multiple comparison test was used to test for statistically significant differences between KN99α cap59Δ, KN99α uge1Δcap59Δ, KN99α uge1Δ and the wild-type strain KN99α (n=3) (ns P > 0.05; * P < 0.05; ** P < 0.01). Histograms show a representative distribution of Crp127 binding for one or all of the strains in the above scatter plot, with the colour-coded key provided for reference. Numerical values in the top left and right of each histogram correspond to the MFI value calculated from the strain labelled directly above.* ***D)*** *R265 cap10Δ,* ***E)*** *B3501 cap67Δ,* ***F)*** *KN99α cap59Δ, uge1Δ, uge1Δcap59Δ and their wild-type strains were labelled for chitin using calcofluor-white (CFW; blue) and Crp127 (far-red; goat Alexa-647-conjugated anti-mouse IgM μ-chain) and maximum-intensity projections*

977 *generated from confocal microscopy z-stacks. Presented are representative images*
978 *merged for transmitted light and Crp127 (left panels) and Crp127 and chitin (right*
979 *panels). Scale bars represent 5 $\mu$m.*
980
981

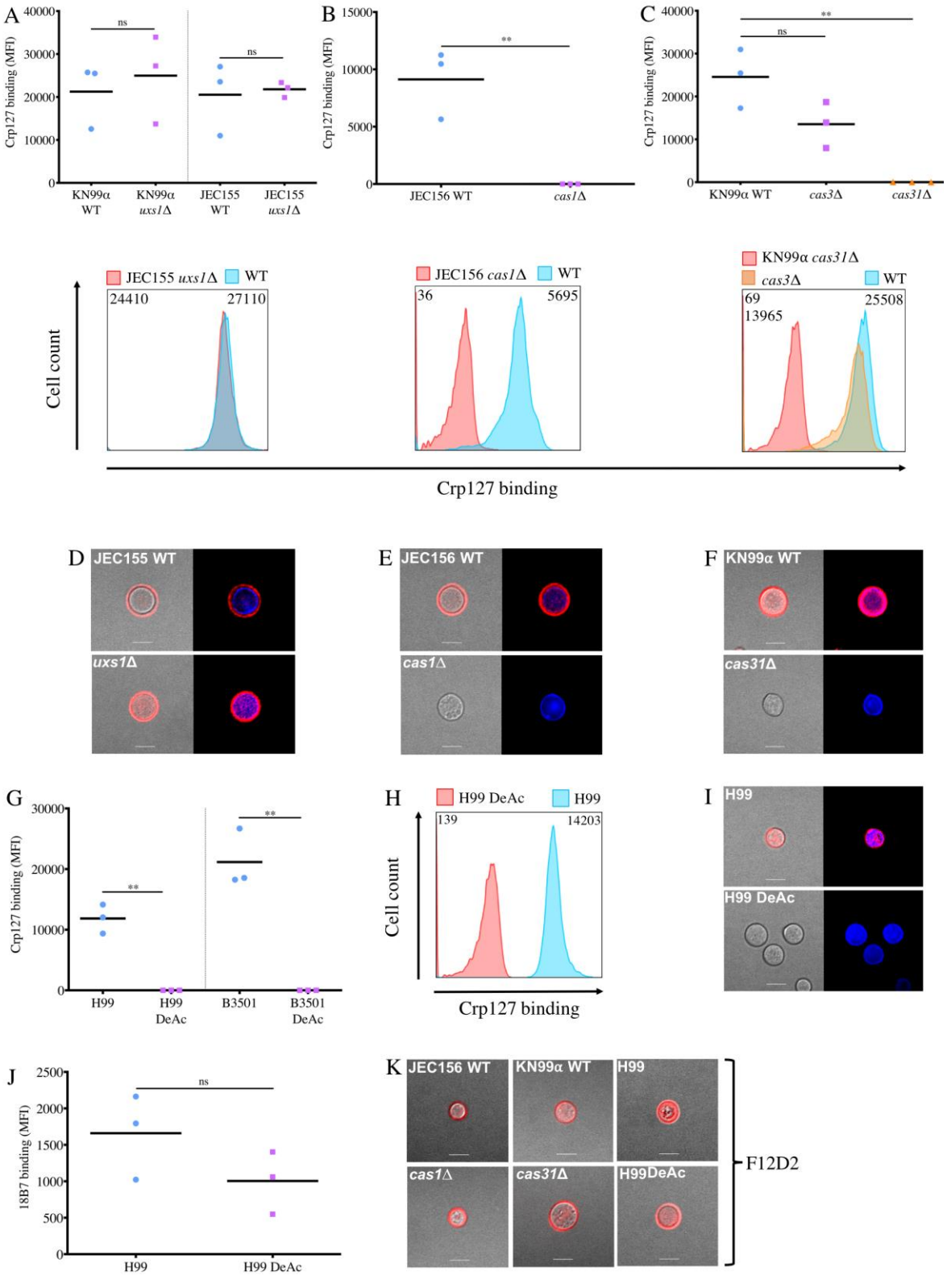
A
Crp127 binding (MFI)
ns
ns
KN99α WT
KN99α uxs1Δ
JEC155 WT
JEC155 uxs1Δ
B
Crp127 binding (MFI)
**
JEC156 WT
cas1Δ
C
Crp127 binding (MFI)
**
ns
KN99α WT
cas3Δ
cas31Δ
JEC155 uxs1Δ
WT
24410
27110
JEC156 cas1Δ
WT
36
5695
KN99α cas31Δ
cas3Δ
WT
69
13965
25508
Cell count
Crp127 binding
D
JEC155 WT
uxs1Δ
E
JEC156 WT
cas1Δ
F
KN99α WT
cas31Δ
G
Crp127 binding (MFI)
**
**
H99
H99 DeAc
B3501
B3501 DeAc
H
H99 DeAc
H99
139
14203
Cell count
Crp127 binding
I
H99
H99 DeAc
J
18B7 binding (MFI)
ns
H99
H99 DeAc
K
JEC156 WT
KN99α WT
H99
cas1Δ
cas31Δ
H99DeAc
F12D2

982

983

984

***Fig. 2. Crp127 requires O-acetylation, but not xylosylation, of GXM for epitope recognition.*** *The ability of Crp127 to recognise mutants with specific defects in GXM modification was quantified via flow cytometry. Scatter plots (top row) and representative histograms (bottom row) are presented for* ***A)*** *KN99α uxs1Δ, JEC155 uxs1Δ and corresponding wild-type strains;* ***B)*** *JEC156 cas1Δ and JEC155 wild-type and* ***C)*** *KN99α cas3Δ, KN99α cas31Δ and KN99α wild-type.* ***D)*** *JEC155 uxs1Δ,* ***E)*** *JEC156 cas1Δ,* ***F)*** *KN99α cas31Δ and corresponding wild-type strains were labelled for chitin and Crp127 imaged via confocal microscopy.* ***G)*** *Binding of Crp127 to chemically deacetylated cells of H99 and B3501 was quantified via flow cytometry with* ***H)*** *a representative histogram presented for H99.* ***I)*** *Untreated (top) and chemically deacetylated (bottom) H99 cells were labelled for chitin and Crp127 and imaged via confocal microscopy.* ***J)*** *Binding of 18B7 to chemically deacetylated cells of H99 and B3501 was quantified via flow cytometry. K) Representative cells from the above strains labelled for chitin (blue) and O-acetyl-independent mAb F12D2 (far-red). For scatter plots, corrected MFI values were calculated by subtracting the MFI value of isotype control cells from the MFI value of the Crp127- or 18B7-treated cells, with data points representing MFI values calculated from three biological replicates performed as independent experiments. A Student's t-test was used to test for statistically significant differences between KN99α uxs1Δ, JEC155 uxs1Δ and JEC156 cas1Δ and their corresponding wild-type strain, as well as between untreated and chemically deacetylated cells of the same strain (n=3). Dunnet's multiple comparison test was used to test for statistically significant differences between KN99α Δcas3, KN99α Δcas31 mutants and the KN99α wild-type strain (n=3) (ns P > 0.05; * P < 0.05; ** P < 0.01). Histograms show a representative distribution of Crp127 or 18B7 binding for one or all of the strains in the above*

*scatter plot, with a colour-coded key provided for reference. Numerical values in the top left and right of each histogram correspond to the MFI value calculated from the strain labelled directly above. Representative maximum intensity projections were merged for transmitted light and Crp127 (far-red), and Crp127 and chitin (blue) (right panels). Scale bars represent 5 μm.*

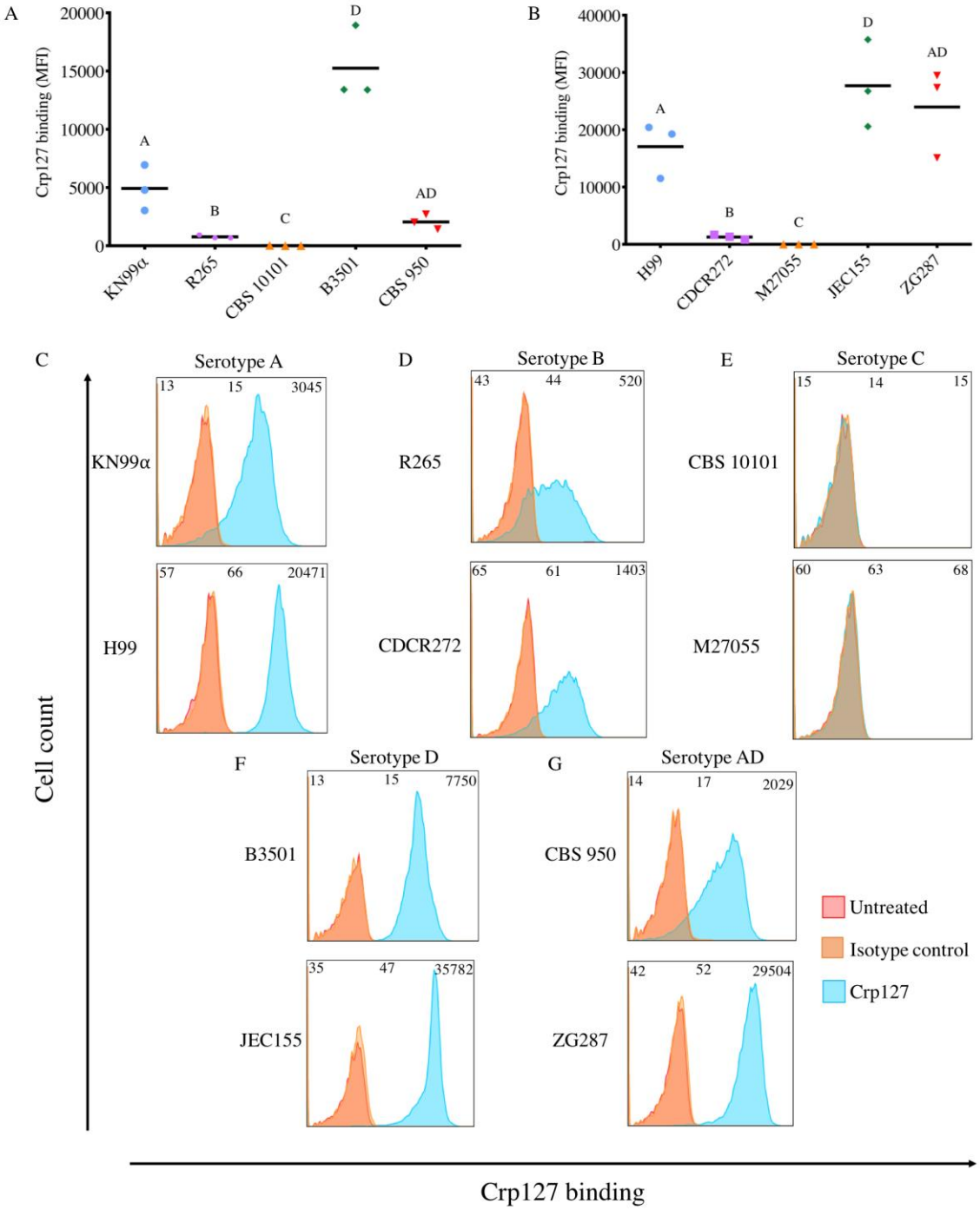
A
Crp127 binding (MFI)
20000
15000
10000
5000
0
A
B
C
D
AD
KN99α
R265
CBS 10101
B3501
CBS 950
B
Crp127 binding (MFI)
40000
30000
20000
10000
0
A
B
C
D
AD
H99
CDCR272
M27055
JEC155
ZG287
C
Serotype A
13
15
3045
KN99α
57
66
20471
H99
D
Serotype B
43
44
520
R265
65
61
1403
CDCR272
E
Serotype C
15
14
15
CBS 10101
60
63
68
M27055
F
Serotype D
13
15
7750
B3501
35
47
35782
JEC155
G
Serotype AD
14
17
2029
CBS 950
42
52
29504
ZG287
Cell count
Crp127 binding
Untreated
Isotype control
Crp127

***Fig. 3. Recognition levels of the Crp127 epitope are associated with serotype.*** *The ability of Crp127 to bind to two different strains from each Cryptococcus serotypes A, B, C, D and AD was quantified using flow cytometry.* ***A-B)*** *Scatter plots show corrected MFI values for each strain, which were calculated by subtracting the MFI value of isotype control cells from the MFI value of the corresponding Crp127-treated cells. Data points represent MFI values calculated from three biological replicates performed as independent experiments (n=3). Histograms show a representative distribution of Crp127 binding for* ***C)*** *serotype A strains KN99$\alpha$ and H99,* ***D)*** *serotype B strains R265 and CDCR272,* ***E)*** *serotype C strains CBS 10101 and M27055,* ***F)*** *serotype D strains B3501 and JEC155 and* ***G)*** *serotype AD hybrid strains CBS 950 and ZG287. Fluorescence intensity values for untreated, isotype control and Crp127-treated cells are presented in red, blue and orange, respectively, with corresponding MFI values displayed in the top left, centre and right of each panel.*

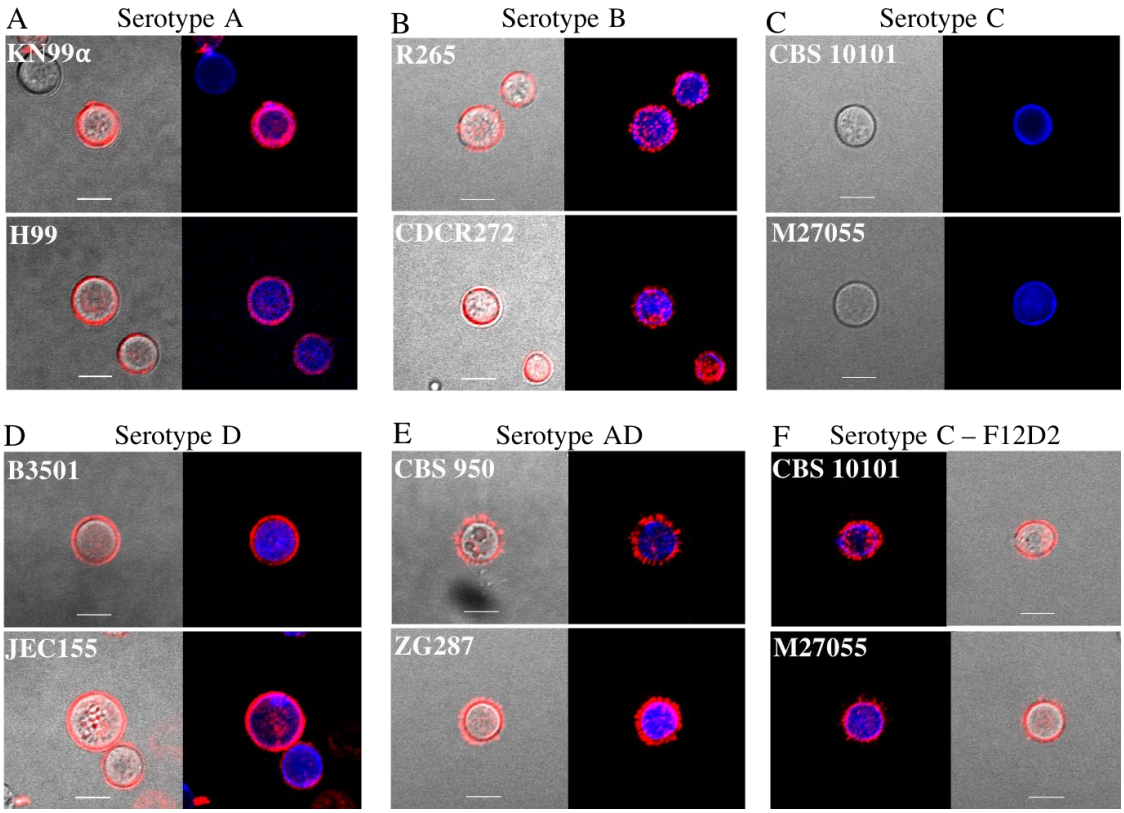
A
Serotype A
KN99α
H99
B
Serotype B
R265
CDCR272
C
Serotype C
CBS 10101
M27055
D
Serotype D
B3501
JEC155
E
Serotype AD
CBS 950
ZG287
F
Serotype C – F12D2
CBS 10101
M27055

***Fig. 4. The immunofluorescence-binding pattern of Crp127 correlates with serotype.*** *Two Cryptococcus strains from* ***A)*** *serotype A (KN99 and H99),* ***B)*** *serotype B (R265 and CDCR272),* ***C)*** *serotype C (CBS 10101 and M27055),* ***D)*** *serotype D (B3501 and JEC155) and* ***E)*** *serotype AD (CBS 950 and ZG287) were labelled for chitin (blue; CFW) and Crp127 (far-red; goat Alexa-647-conjugated anti-mouse IgM $\mu$-chain). F) Representative cells from serotype C strains CBS 10101 and M27055 labelled for chitin (blue) and O-acetyl-independent mAb F12D2 (far-red; Alexa-647-conjugated F(ab')2 goat anti-Mouse IgG (H+L)). Maximum-intensity projections were generated via confocal microscopy. Representative images are shown for each strain. Images are merged for transmitted light and Crp127 (left panels) and Crp127 and chitin (right panels). Scale bars represent 5 $\mu$m.*

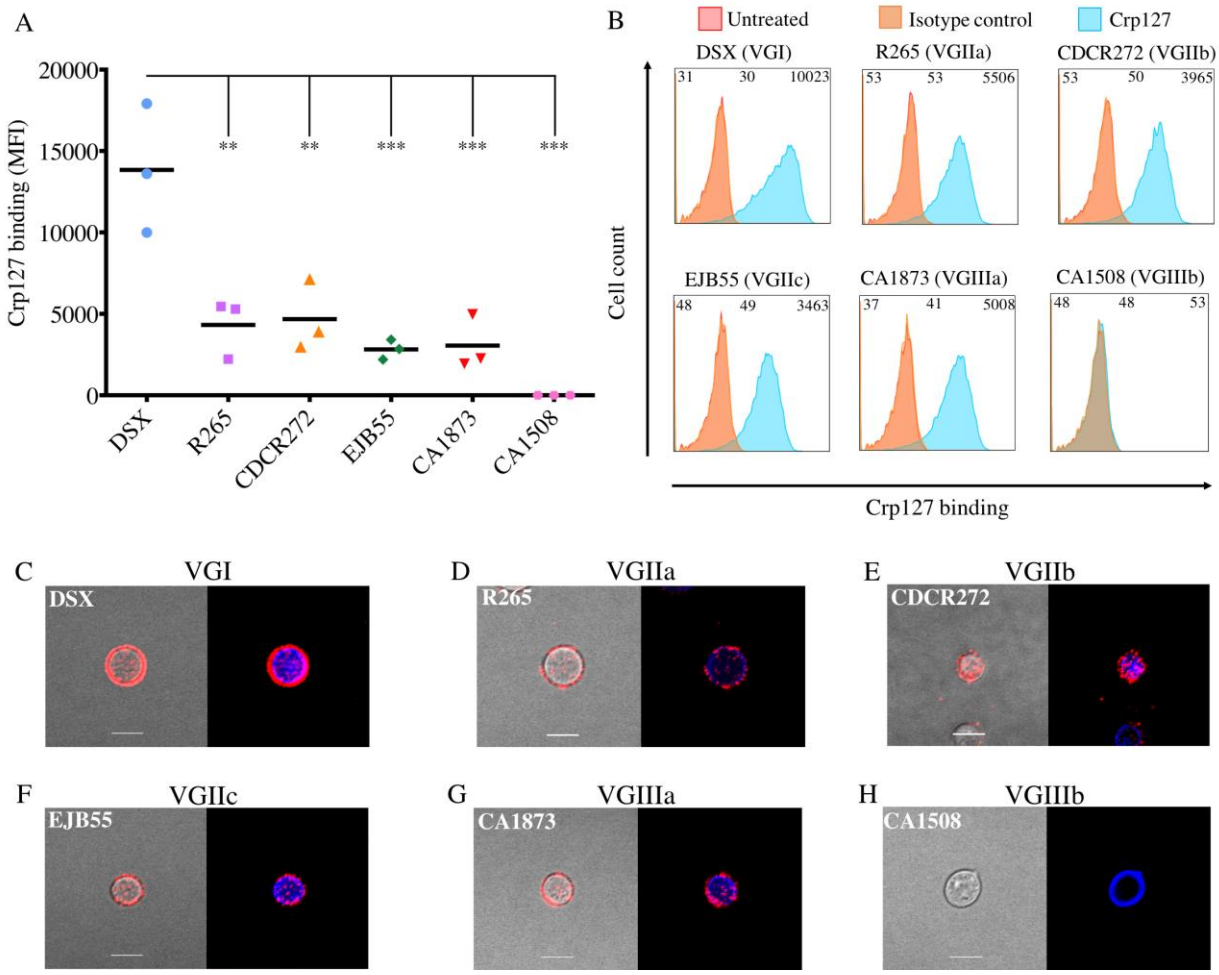
A
Crp127 binding (MFI)
20000
15000
10000
5000
0
**
**
***
***
***
DSX
R265
CDCR272
EJB55
CA1873
CA1508
B
Untreated
Isotype control
Crp127
DSX (VGI)
31 30 10023
R265 (VGIIa)
53 53 5506
CDCR272 (VGIIb)
53 50 3965
EJB55 (VGIIc)
48 49 3463
CA1873 (VGIIIa)
37 41 5008
CA1508 (VGIIIb)
48 48 53
Cell count
Crp127 binding
C
VGI
DSX
D
VGIIa
R265
E
VGIIb
CDCR272
F
VGIIc
EJB55
G
VGIIIa
CA1873
H
VGIIIb
CA1508

***Fig. 5. Recognition of the Crp127 epitope is largely consistent within C. gattii serotypes.*** *The ability of Crp127 to bind to six strains from C. gattii that encompass molecular types VGI-VGIIIb was quantified via flow cytometry.* ***A)*** *Scatter plots show corrected MFI values for each strain, which were calculated by subtracting the MFI value of isotype control cells from the MFI value of the corresponding Crp127-treated cells. Data points represent MFI values calculated from three biological replicates performed as independent experiments. Tukey's multiple comparisons test was used to test the statistical significance of differences between the six strains (n=3) (ns P > 0.05; ** P < 0.01; *** P < 0.001).* ***B)*** *Histograms show a representative distribution of Crp127 binding for strains DSX (VGI), R265 (VGIIa), CDCR272 (VGIIb), EJB55 (VGIIc), CA1873 (VGIIIa) and CA1508 (VGIIIb). Fluorescence intensity values for untreated, isotype control and Crp127-treated cells are presented in red, blue and orange, respectively, with corresponding MFI values displayed in the top left, centre and right of each panel. C. gattii strains* ***C)*** *DSX,* ***E)*** *R265,* ***F)*** *CDCR272,* ***G)*** *CA1873 and* ***H)*** *CA1508 were labelled for chitin (blue; CFW) and Crp127 (far-red; goat Alexa-647-conjugated anti-mouse IgM $\mu$-chain) and maximum-intensity projections generated via confocal microscopy. Presented are representative images merged for transmitted light and Crp127 (left panels) and Crp127 and chitin (right panels). Scale bars represent 5 $\mu$m.*

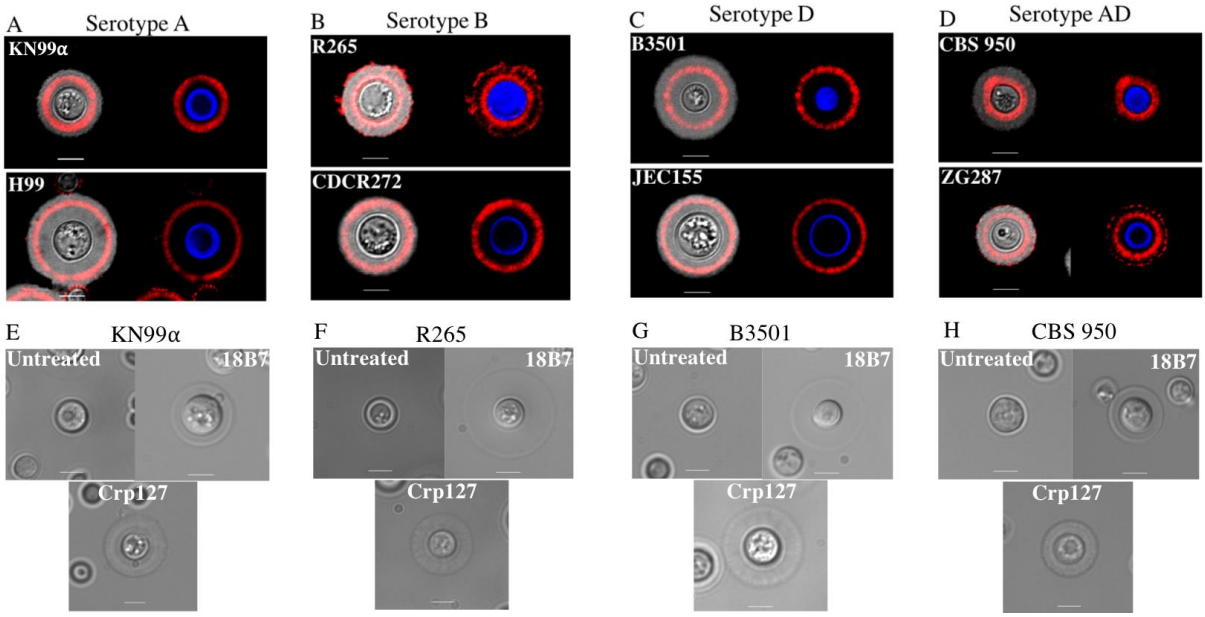
A
Serotype A
KN99α
H99
B
Serotype B
R265
CDCR272
C
Serotype D
B3501
JEC155
D
Serotype AD
CBS 950
ZG287
E
KN99α
Untreated
18B7
Crp127
F
R265
Untreated
18B7
Crp127
G
B3501
Untreated
18B7
Crp127
H
CBS 950
Untreated
18B7
Crp127

***Fig. 6. The Crp127 epitope is spatially confined to distinct capsular regions and binding elicits capsular swelling reactions distinct from those of 18B7.*** *Cryptococcus cells were grown in capsule-inducing conditions and imaged to determine the location of the Crp127 epitope within the enlarged capsule and characterise the capsular reaction patterns elicited by this antibody. Cryptococcus strains from* ***A)*** *serotype A (KN99$\alpha$ and H99),* ***B)*** *serotype B (R265 and CDCR272,* ***C)*** *serotype D (B3501 and JEC155) and* ***D)*** *serotype AD (CBS 950 and ZG287) were labelled for chitin (blue; CFW) and Crp127 (far-red; goat Alexa-647-conjugated anti-mouse IgM $\mu$-chain), suspended in Indian ink to visualise the capsule and imaged using confocal microscopy. Representative images of a single focal plane are shown for each strain. Presented are images merged for transmitted light and Crp127 (left panels) and Crp127 and chitin (right panels). Capsule-induced cells of strains* ***E)*** *KN99$\alpha$,* ***F)*** *R265,* ***G)*** *B3501 and* ***H)*** *CBS 950 were also left untreated (top right panels), treated with mAb 18B7 (top right panels) or with mAb Crp127 (bottom panels) and imaged using DIC microscopy to observe capsular reaction patterns. Scale bars represent 5 $\mu$m.*

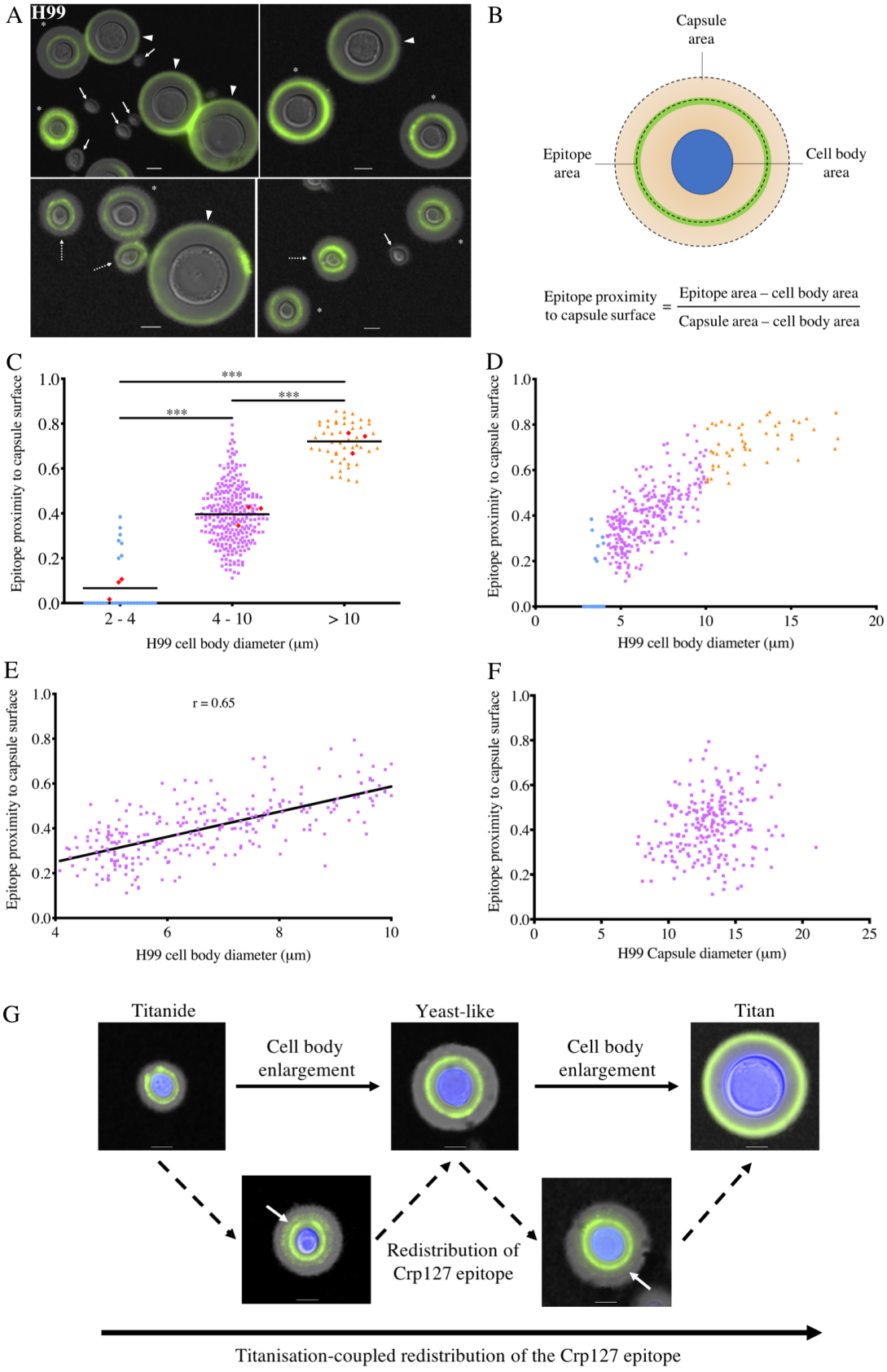
A
H99
B
Capsule area
Epitope area
Cell body area
Epitope proximity to capsule surface = Epitope area – cell body area / Capsule area – cell body area
C
Epitope proximity to capsule surface
***
***
***
2 - 4
4 - 10
> 10
H99 cell body diameter (μm)
D
Epitope proximity to capsule surface
H99 cell body diameter (μm)
E
r = 0.65
Epitope proximity to capsule surface
H99 cell body diameter (μm)
F
Epitope proximity to capsule surface
H99 Capsule diameter (μm)
G
Titanide
Cell body enlargement
Yeast-like
Cell body enlargement
Titan
Redistribution of Crp127 epitope
Titanisation-coupled redistribution of the Crp127 epitope

1186

1187

***Fig. 7. Spatial distribution of the Crp127 epitope differs within the capsule of the three cell subtypes found in Titanising populations of strain H99, suggesting a model of Titanisation-coupled epitope redistribution****. Cultures of C. neoformans strain H99 that derived solely from Titan cells were investigated for differences in the capsular distribution of the Crp127 epitope.* ***A)*** *Representative images of cells from strain H99 grown under conditions permissive for Titanisation, resulting in formation of Titanide (block arrows and dashed arrows distinguish no Crp127 binding and binding, respectively), yeast-like (asterisks) and Titan cells (arrowheads).* ***B)*** *A schematic representation of how Crp127 epitope proximity to the capsule surface was quantified through the analysis of micrographs using ImageJ. Where no antibody binding was detected, the ratio was calculated as 0.* ***C)*** *The proximity of the Crp127 epitope to the capsule surface of 2-4 μm, 4-10 μm and >10 μm cells of strain H99 was quantified. Data points represent all individual cells for which the location of the Crp127 epitope was quantified, whilst the horizontal bar represents the mean of pooled cells. Red diamonds represent mean values calculated from each of three biological repeats. Tukey's multiple comparisons test was used to test for statistically significant differences between the three groups (n=3) (** P < 0.01; *** P < 0.001).* ***D****) Cell body diameter was plotted against the epitope proximity to the capsule surface for all cells measured and from* ***E)*** *cells 4-10 μm in cell body diameter.* ***F)*** *Capsule diameter was plotted against the epitope proximity to the capsule surface for cells 4-10 μm in cell body diameter.* ***G)*** *Model for Titanisation-coupled redistribution of the Crp127 epitope. Presented are representative images of Titanide, yeast-like and Titan cells (top row) of strain H99 that were recognised by Crp127, in addition to Titanide and yeast-like cells exhibiting*

*a second faint ring of antibody binding (white arrows) (bottom row). Scale bars represent 5 $\mu$m.*

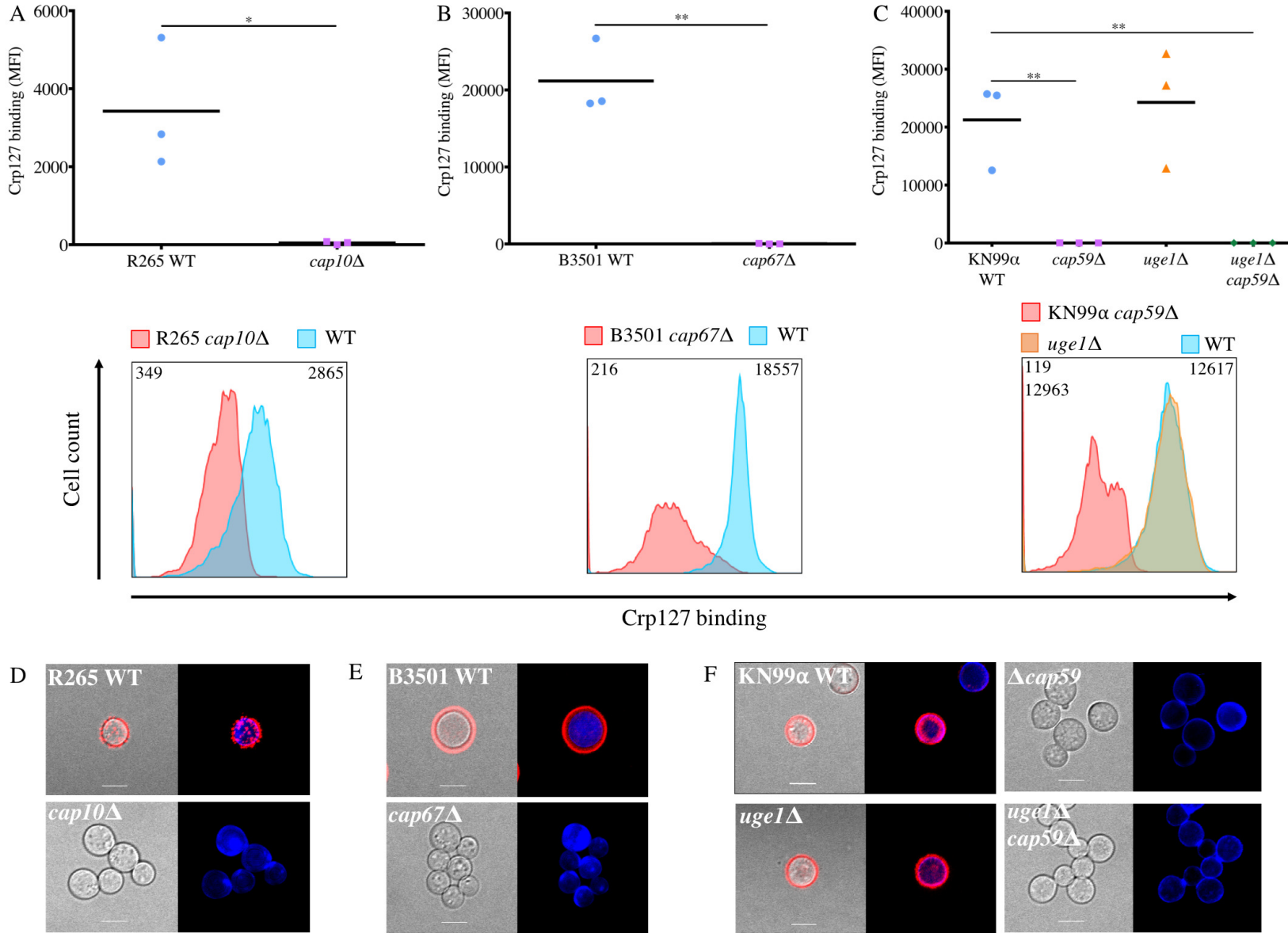
A
Crp127 binding (MFI)
6000
4000
2000
0
*
R265 WT
cap10Δ
B
Crp127 binding (MFI)
30000
20000
10000
0
**
B3501 WT
cap67Δ
C
Crp127 binding (MFI)
40000
30000
20000
10000
0
**
**
KN99α WT
cap59Δ
uge1Δ
uge1Δ cap59Δ
R265 cap10Δ
WT
349
2865
B3501 cap67Δ
WT
216
18557
KN99α cap59Δ
uge1Δ
WT
119
12963
12617
Cell count
Crp127 binding


D
R265 WT
cap10Δ
E
B3501 WT
cap67Δ
F
KN99α WT
Δcap59
uge1Δ
uge1Δ cap59Δ

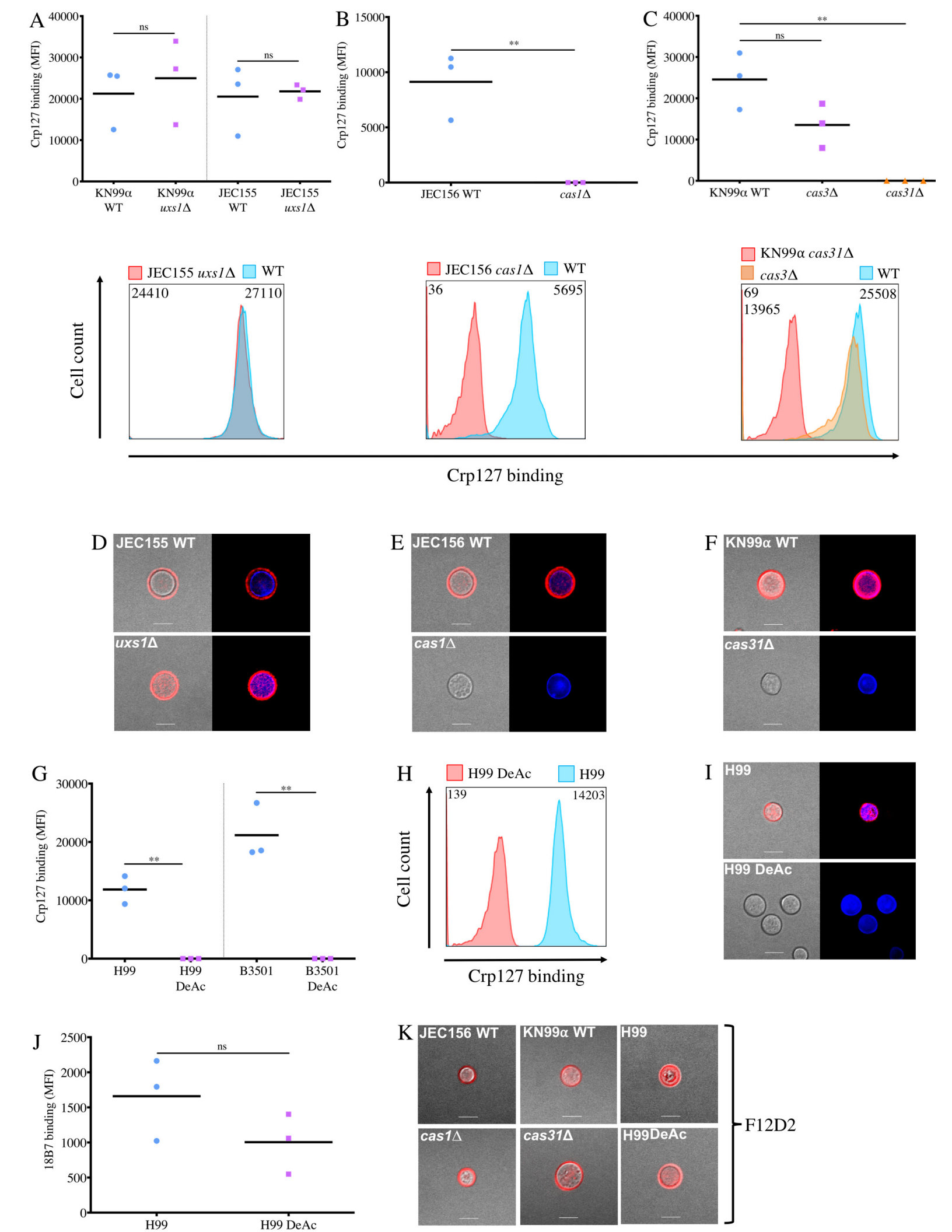
A
Crp127 binding (MFI)
40000
30000
20000
10000
0
ns
ns
KN99α WT
KN99α uxs1Δ
JEC155 WT
JEC155 uxs1Δ
B
Crp127 binding (MFI)
15000
10000
5000
0
**
JEC156 WT
cas1Δ
C
Crp127 binding (MFI)
40000
30000
20000
10000
0
**
ns
KN99α WT
cas3Δ
cas31Δ
JEC155 uxs1Δ
WT
24410
27110
JEC156 cas1Δ
WT
36
5695
KN99α cas31Δ
cas3Δ
WT
69
13965
25508
Cell count
Crp127 binding
D
JEC155 WT
uxs1Δ
E
JEC156 WT
cas1Δ
F
KN99α WT
cas31Δ
G
Crp127 binding (MFI)
30000
20000
10000
0
**
**
H99
H99 DeAc
B3501
B3501 DeAc
H
H99 DeAc
H99
139
14203
Cell count
Crp127 binding
I
H99
H99 DeAc
J
18B7 binding (MFI)
2500
2000
1500
1000
500
0
ns
H99
H99 DeAc
K
JEC156 WT
KN99α WT
H99
cas1Δ
cas31Δ
H99DeAc
F12D2

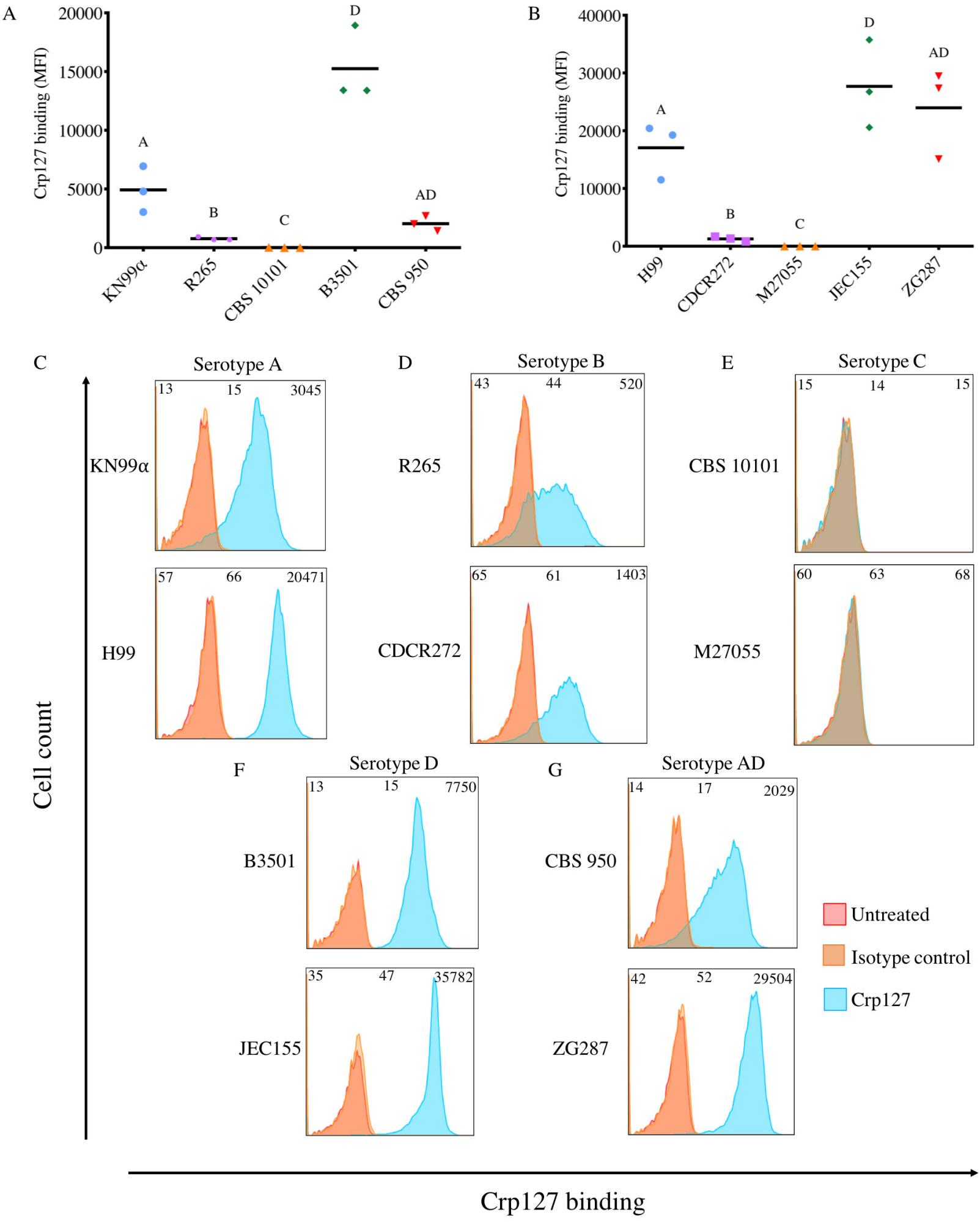
A
Crp127 binding (MFI)
20000
15000
10000
5000
0
A
B
C
D
AD
KN99α
R265
CBS 10101
B3501
CBS 950
B
Crp127 binding (MFI)
40000
30000
20000
10000
0
A
B
C
D
AD
H99
CDCR272
M27055
JEC155
ZG287
C
Serotype A
KN99α
13
15
3045
H99
57
66
20471
D
Serotype B
R265
43
44
520
CDCR272
65
61
1403
E
Serotype C
CBS 10101
15
14
15
M27055
60
63
68
F
Serotype D
B3501
13
15
7750
JEC155
35
47
35782
G
Serotype AD
CBS 950
14
17
2029
ZG287
42
52
29504
Untreated
Isotype control
Crp127
Cell count
Crp127 binding

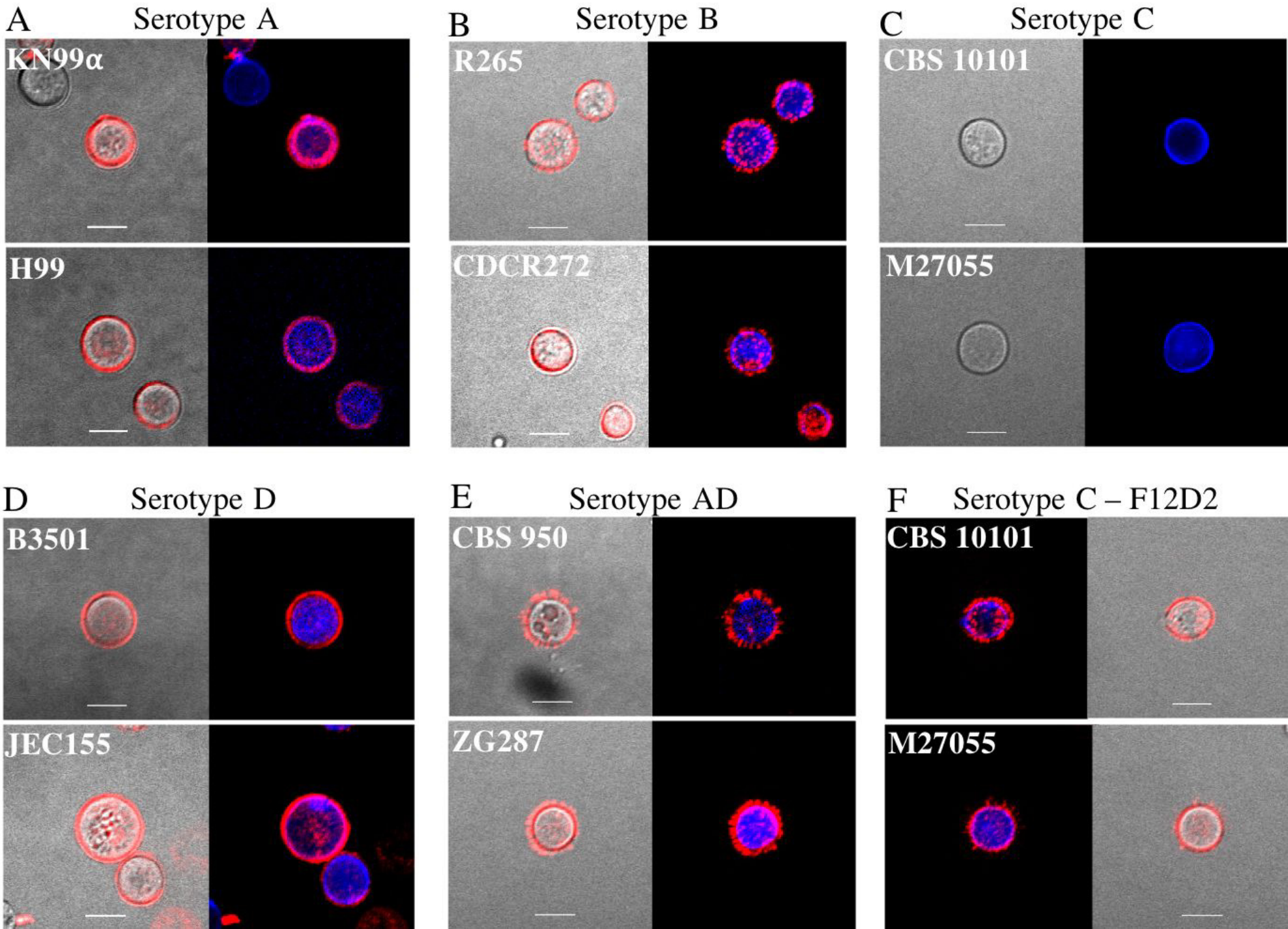
A
Serotype A
KN99α
H99
B
Serotype B
R265
CDCR272
C
Serotype C
CBS 10101
M27055
D
Serotype D
B3501
JEC155
E
Serotype AD
CBS 950
ZG287
F
Serotype C – F12D2
CBS 10101
M27055

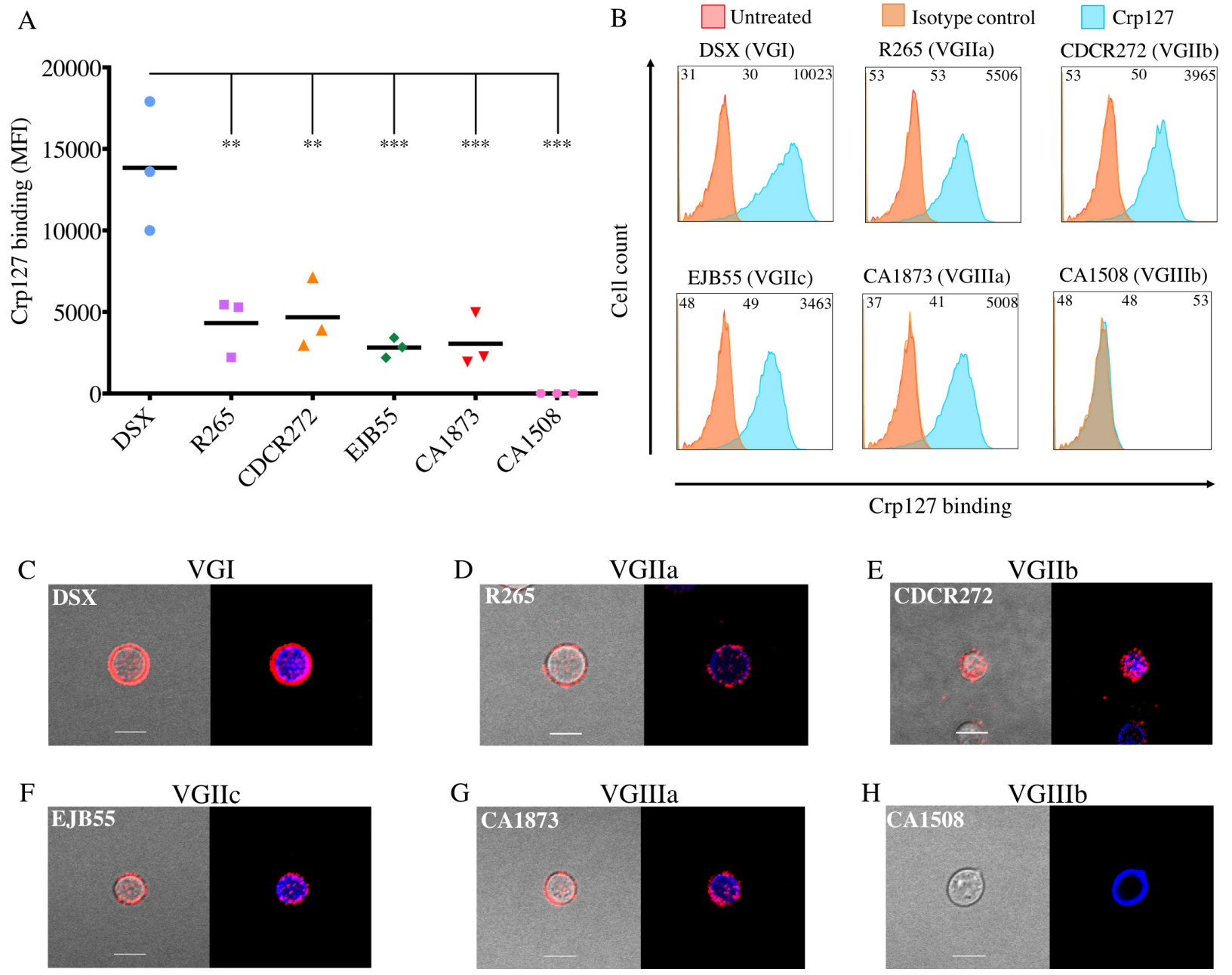
A
Crp127 binding (MFI)
20000
15000
10000
5000
0
**
**
***
***
***
DSX
R265
CDCR272
EJB55
CA1873
CA1508
B
Untreated
Isotype control
Crp127
DSX (VGI)
31
30
10023
R265 (VGIIa)
53
53
5506
CDCR272 (VGIIb)
53
50
3965
EJB55 (VGIIc)
48
49
3463
CA1873 (VGIIIa)
37
41
5008
CA1508 (VGIIIb)
48
48
53
Cell count
Crp127 binding
C
VGI
DSX
D
VGIIa
R265
E
VGIIb
CDCR272
F
VGIIc
EJB55
G
VGIIIa
CA1873
H
VGIIIb
CA1508

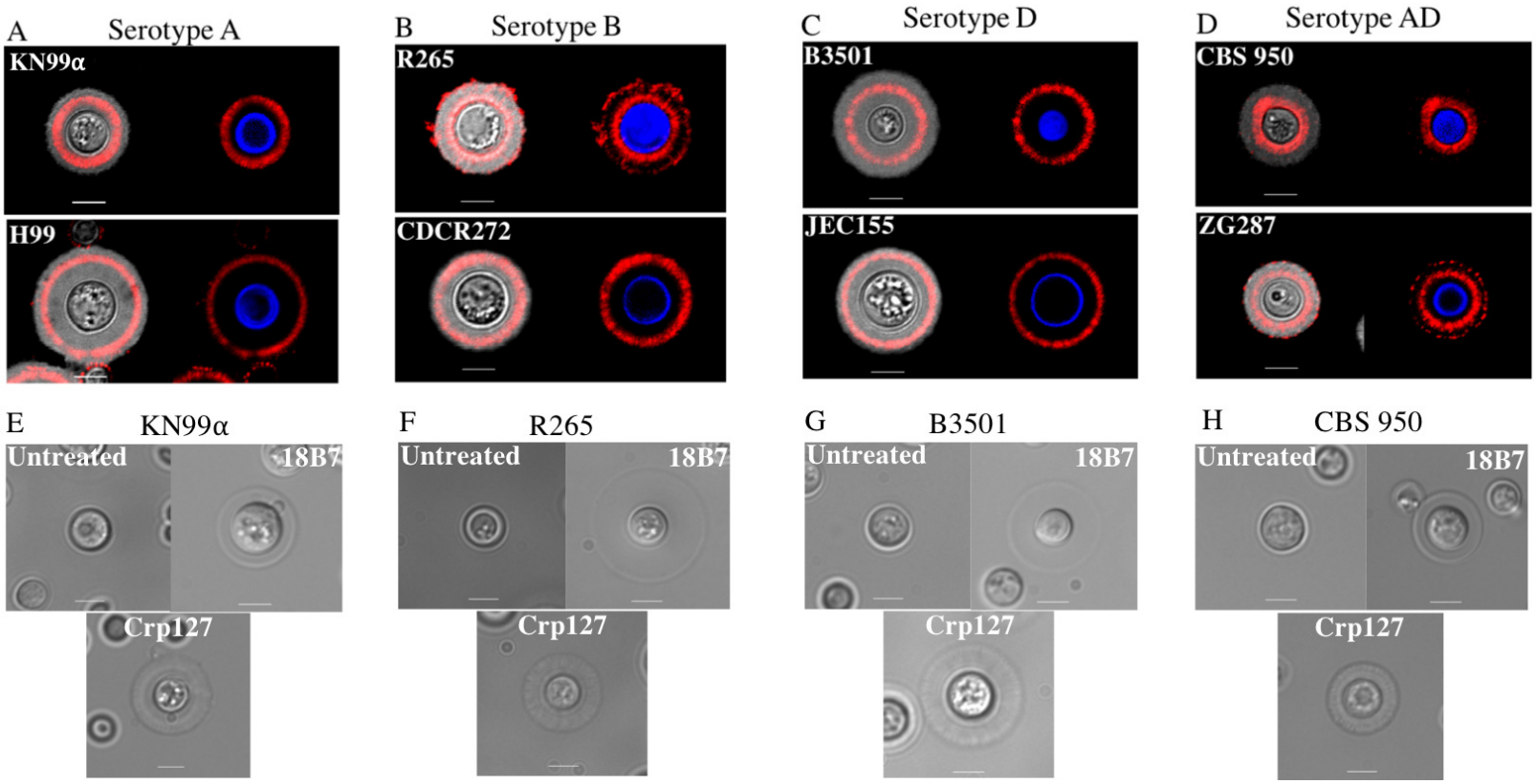
A
Serotype A
KN99α
H99
B
Serotype B
R265
CDCR272
C
Serotype D
B3501
JEC155
D
Serotype AD
CBS 950
ZG287
E
KN99α
Untreated
18B7
Crp127
F
R265
Untreated
18B7
Crp127
G
B3501
Untreated
18B7
Crp127
H
CBS 950
Untreated
18B7
Crp127

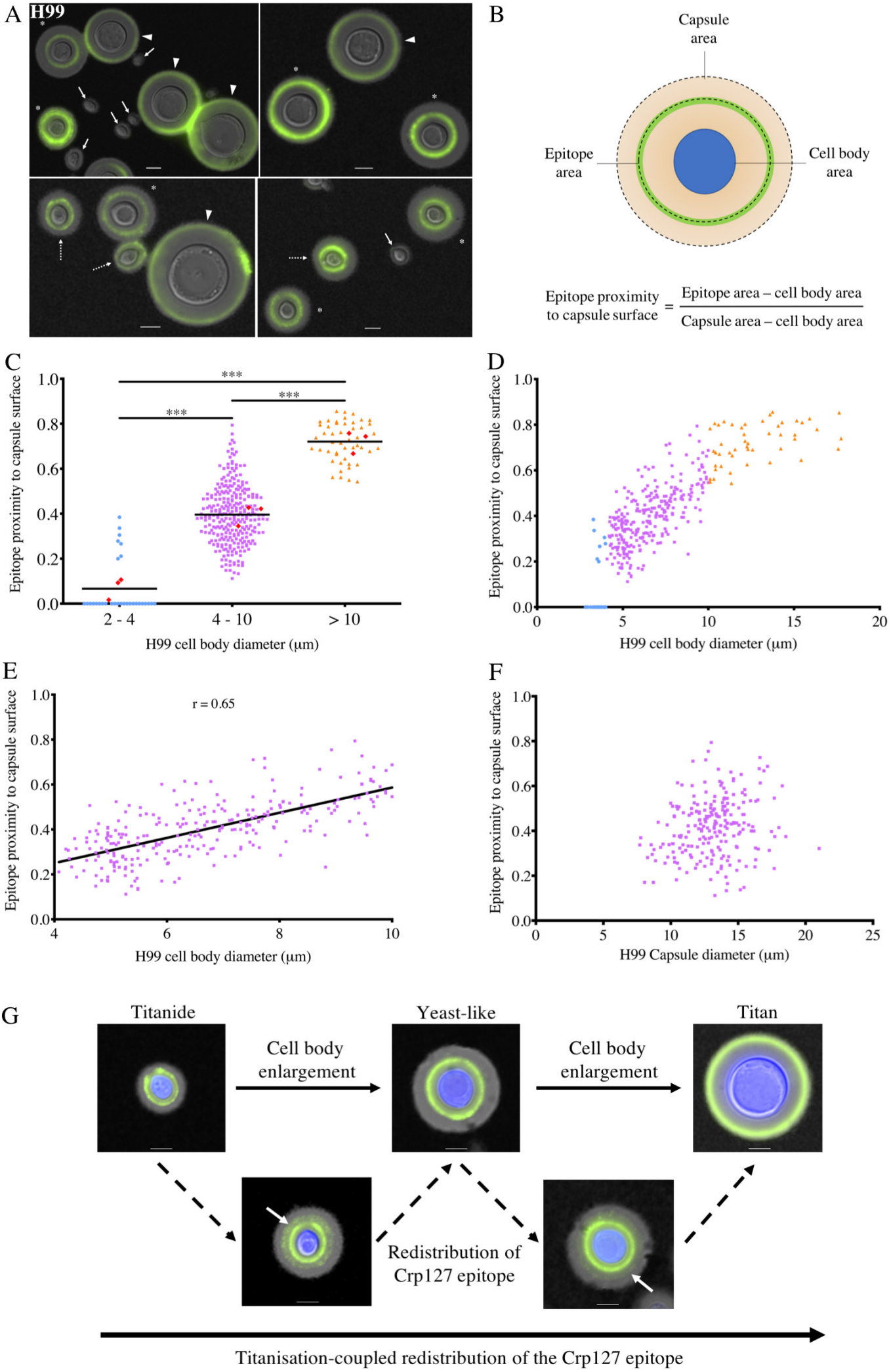
A
H99
B
Capsule area
Epitope area
Cell body area
Epitope proximity to capsule surface = Epitope area – cell body area / Capsule area – cell body area
C
Epitope proximity to capsule surface
***
***
***
2 - 4
4 - 10
> 10
H99 cell body diameter (µm)
D
Epitope proximity to capsule surface
H99 cell body diameter (µm)
E
r = 0.65
Epitope proximity to capsule surface
H99 cell body diameter (µm)
F
Epitope proximity to capsule surface
H99 Capsule diameter (µm)
G
Titanide
Cell body enlargement
Yeast-like
Cell body enlargement
Titan
Redistribution of Crp127 epitope
Titanisation-coupled redistribution of the Crp127 epitope